For Reference

NOT TO BE TAKEN FROM THIS ROOM

For Reference

NOT TO BE TAKEN FROM THIS ROOM

Ex libris universitatis albertaensis

UNIVERSITY OF ALBERTA

QUAECUMQUE VERA

University of Alberta
Printing Department

Digitized by the Internet Archive
in 2019 with funding from
University of Alberta Libraries

https://archive.org/details/effectofmagnetic00john

Thesis
1963
10

THE UNIVERSITY OF ALBERTA

THE EFFECT OF A MAGNETIC FIELD ON THE SOLIDIFICATION OF ALUMINUM - COPPER ALLOYS

by

John Raymond Cahoon

A THESIS

SUBMITTED TO THE FACULTY OF GRADUATE STUDIES

IN PARTIAL FULFILMENT OF THE REQUIREMENTS FOR THE DEGREE

OF MASTER OF SCIENCE

DEPARTMENT OF MINING AND METALLURGY

EDMONTON, ALBERTA

APRIL 1963

ABSTRACT

The effect of a magnetic field on the solidification of aluminum(rich)- copper alloys was studied using the maximum inverse segregation at the chill face as a criterion. Field strengths ranged from 0 to 34,000 oersteds and the effects of fields both parallel and perpendicular to the direction of solidification were studied. The "field" solidified ingots, compared to "no field" ingots, showed an increase in inverse segregation; the amount of segregation increased with increasing field strength and was 60% higher than "no field" results at a field of 34,000 oersteds. A theory has been developed which qualitatively agrees with the results in the Al - Cu system as well as in other systems which have been studied.

ACKNOWLEDGEMENTS

The author is very grateful for the guidance and supervision of Dr. W. V. Youdelis during the course of this project. He would also like to thank Professor E. O. Lilge for his helpful departmental supervision and Mr. R. M. Scott who assisted with the metallography. The author is also indebted to the many staff members and students of the department for their helpful discussions and criticisms, especially to Mr. D. R. Colton, MSc., and Mr. M. J. Bibby, BSc., who helped in so many ways.

The financial assistance provided by the Steel Company of Canada and the National Research Council are gratefully acknowledged.

TABLE OF CONTENTS

Page

I INTRODUCTION 1

II THEORETICAL

A GENERAL 3

B SOLIDIFICATION OF PURE METALS 8

C SOLIDIFICATION OF BINARY ALLOYS

1. Solute Distribution 9

a) Very Slow Solidification 9

b) Slow or "Normal" Solidification 11

c) Rapid Solidification 13

d) Exudations 17

2. Macrostructure of Binary Alloys 17

III EXPERIMENTAL

A APPARATUS

1. The Magnets 21

2. Casting Unit 21

B METHOD 24

C ANALYSIS 26

Page

IV RESULTS

A METALLOGRAPHIC 27

B SEGREGATION 27

V DISCUSSION

A CRYSTAL MORPHOLOGY 42

B SEGREGATION 42

VI THEORY OF MAGNETIC EFFECTS

A THERMODYNAMIC CONSIDERATIONS 45

B THE PLASMA CONCEPT OF A METAL 47

C DIFFUSION INHIBITION AND ITS CONSEQUENCES 49

D ENERGY CONSIDERATIONS 51

VII SUMMARY AND CONCLUSIONS 55

BIBLIOGRAPHY 56

APPENDIX 58

ILLUSTRATIONS AND FIGURES

Figure Page

1. Atomic positions in a close-packed surface , the (111) surface for a face-centered cubic crystal . 6.
2. Rates of solidifying and melting for copper . 7.
3. Schematic drawing of the surface of a crystal, growing by the edgewise extension of close-packed planes . 7.
4. The distribution coefficient, $K_0 = \frac{C_S}{C_L}$. 10.
5. Solidification for $k_0 < 1$ 10.
6. Solute distribution in the solid for the case of complete mixing in the liquid . 12.
7. Concentration gradient in the liquid at the interface . 12.
8. Solute distribution in the solid for slow solidification when transport in the liquid is by diffusion only. 14.
9. Constitutional supercooling ahead of an advancing solid - liquid interface . 14.
10. Solute distribution for inverse segregation . 16.
11. Massive exudations caused by remelting . 16.
12. Exudations caused by surface tension forces . 18.
13. Solenoid magnet and solidification apparatus . 22.
14. Pole-type electromagnet . 23.

Figure Page

15. Schematic diagram of casting unit. 25.

16. Macrostructure of an Al - 10% Cu ingot cast in zero field (XI). 28.

17. Macrostructure of an Al - 10% Cu ingot cast in a field of 13,000 oersteds applied parallel to the direction of solidification (XI). 28.

18. Macrostructure of an Al - 10% Cu ingot cast in a field of 34,000 oersteds applied perpendicular to the direction of solidification (XI). 29.

19. Microstructure of Al - 10% Cu ingot cast in zero field (X100). 29.

20. Microstructure of Al - 10% Cu ingot solidified in a parallel field of 13,000 oersteds (X100). 30.

21. Microstructure of Al - 10% Cu ingot solidified in a perpendicular field of 34,000 oersteds (X100). 30.

22. Macrostructure of Al - 20% Cu ingot solidified in a field of 34,000 oersteds (XI). 31.

23. Macrostructure of Al - 5% Cu ingot solidified in a perpendicular field of 34,000 oersteds (XI). 31.

24. Microstructure of Al - 20% Cu ingot solidified in a perpendicular field of 34,000 oersteds(X100). 32.

25. Microstructure of Al - 5% Cu ingot solidified in a perpendicular field of 34,000 oersteds (X100). 32.

26. Maximum segregation in the Al - Cu system for field strengths of 13,000 and 34,000 oersteds. 34.

Figure Page

27. Effect of field strength on maximum segregation in Al - 10% Cu ingots. 36.

28. Base analysis of an Al - 9.27 Cu ingot showing extrapolation correcting for exudations and finite sample size. 37.

29. Base analysis of an Al - 19.04% Cu ingot showing extrapolation correcting for exudations and finite sample size. 38.

30. Base analysis of an ingot which had no exudations. 39.

31. Microstructure of an Al - 10% Cu ingot cast in a perpendicular field of 13,000 oersteds showing the absence of exudations (X200). 40.

32. Comparison of field and no-field cooling curves for Al - 10% Cu ingots. 41.

33. Constitutional diagram and specific volume relationships for the aluminum (rich) - copper system. 44.

34. Concentration gradients and temperature distributions at the solid - liquid interface. 50.

INDEX OF TABLES

Table #1 Analysis of Ingots 33.

I INTRODUCTION

The successful application of a magnetic field in studying the electronic structure and transport properties of solids, such as, for example, the phenomena of galvanomagnetism, thermomagnetism and the Hall effect, suggests that a magnetic field may also provide a powerful tool in studying the electronic structure of liquid metals and their alloys, and the mechanisms of solidification. With this in mind, a study was made of the effect of a magnetic field on segregation phenomena occuring during solidification in ingots of aluminum (rich) - copper alloys.

Maximum inverse segregation occuring at the chill face of the ingot was selected as the principal criterion for determining the effect of the magnetic field because the amount of segregation, which is readily determined by ordinary chemical analysis, is related directly to the constitutional - specific volume relationship of the alloy system. Any change in this relationship which may be effected by the magnetic field will be readily indicated by a change in the amount of inverse segregation.

Previous work by D. R. Colton (1) on the solidification of binary alloys of the bismuth (rich) - tin and bismuth - antimony systems in a magnetic field of 13,000 oersteds, applied parallel to the direction of solidification, indicated that the field changed the amount of inverse segregation by about + 70% and -100% respectively over the "no-field" results. To establish whether the change in

segregation due to the field may be a result of the high diamagnetic susceptibility of bismuth and its alloys, it was decided to study this effect in alloys of the aluminum (rich) - copper system which has a relatively low paramagnetic susceptibility. Two other reasons for choosing the alloys of the aluminum (rich) - copper system for study were:

(1) the "no field" segregation results in the aluminum-copper system are already well established,(2) and

(2) the relatively large difference in the valencies of the solvent and solute metals.

The latter point may be important if, as suspected, the effect of the field on segregation is via the transport mechanisms involved in solidification, principally that of diffusion.

II THEORETICAL

The following is a resume of the theory of solidification for both pure metals and binary alloys. Solute distribution for various rates of solidification of binary alloys is also considered.

A. GENERAL

In studying solidification the solid - liquid interface is the region of greatest interest. On one side of the interface exists a crystalline solid wherein each atom has a well defined position and, on the other side, there is liquid wherein the atoms are about as far apart as in the solid but the arrangement is much less systematic and is continuously changing. The average energy of the atoms in the liquid is greater than that of the atoms in the solid by an amount equal to the latent heat of fusion. Chalmers(3) suggests that there is a continuous and rapid exchange of atoms between solid and liquid at the solid - liquid interface, and that during solidification the net result is more atoms are leaving the liquid and joining the solid than for the reverse process which constitutes melting.

Chalmers(3) assumes that an atom will cross the solid - liquid interface if it has energy in excess of some value which is higher than the average value in either the solid or liquid. The average energy of the atoms varies with the temperature but the actual energies are distributed about the average energy such that the fraction

of atoms having an energy equal to or in excess of energy Q is given by:

$$f = e^{-Q/RT} \qquad (1)$$

If an atom vibrates ν times per second, then on the average it will have energy Q or greater $\nu e^{-Q/RT}$ times per second. There are, however, two reasons why an atom having the required energy may not cross the interface:

(1) the atom may not be vibrating in the proper direction i.e., it may not have the required velocity perpendicular to the interface, and

(2) the atom may not be accommodated onto the other side of the interface.

If the probability of vibration in the right direction is G and the probability of being accommodated on the other side of the interface is A, then the rate of solidification is given by:

$$R_S = A_S G_S \nu e^{-Q_s/RT} \qquad (2)$$

and the rate of melting is given by:

$$R_m = A_m G_m \nu e^{-Q_m/RT} \qquad (3)$$

where the subscripts "S" and "m" refer to solidifying and melting respectively. If E_A is the energy required to cross the interface and E_S and E_L are the binding energies of the solid and liquid respectively, then

$$Q_S = E_A - E_L$$

and $$Q_m = E_A - E_S$$

Also, Q_s should be equal to the activation energy for diffusion in the liquid and $Q_m - Q_s$ should be equal to the latent heat of fusion.

The accommodation coefficients are related by the equation,

$$\frac{A_m}{A_s} = e^{-H/RT_e}$$

where H is the latent heat of fusion and T_e is the solidification temperature. "A_m" should be the same for all monatomic liquids and "A_s" should depend upon the crystal structure at the interface. More explicitly, there are only certain available sites where an atom from the liquid may settle on the interface and join the solid. For example, Figure 1 represents the atomic positions of the (111) plane of a face centered cubic crystal. The shaded areas represent the sites for an approaching atom from the liquid. The shaded area is about 10% of the total area and, therefore, A_s should be about 0.10 for the (111) plane of a f.c.c. metal. Similar arguments hold for determining the accommodation coefficients of other planes for other crystalline structures.

Chalmers(3) has calculated the rates of freezing and melting for copper applying the foregoing theory and the results are shown in Figure 2. The calculated rates of freezing and melting at the equilbirium temperature are 3,000 centimeters per second. The observed rate of freezing at a reasonable degree of supercooling, say 50°C, would be 25 cm. per second which seems reasonable for this degree of supercooling.

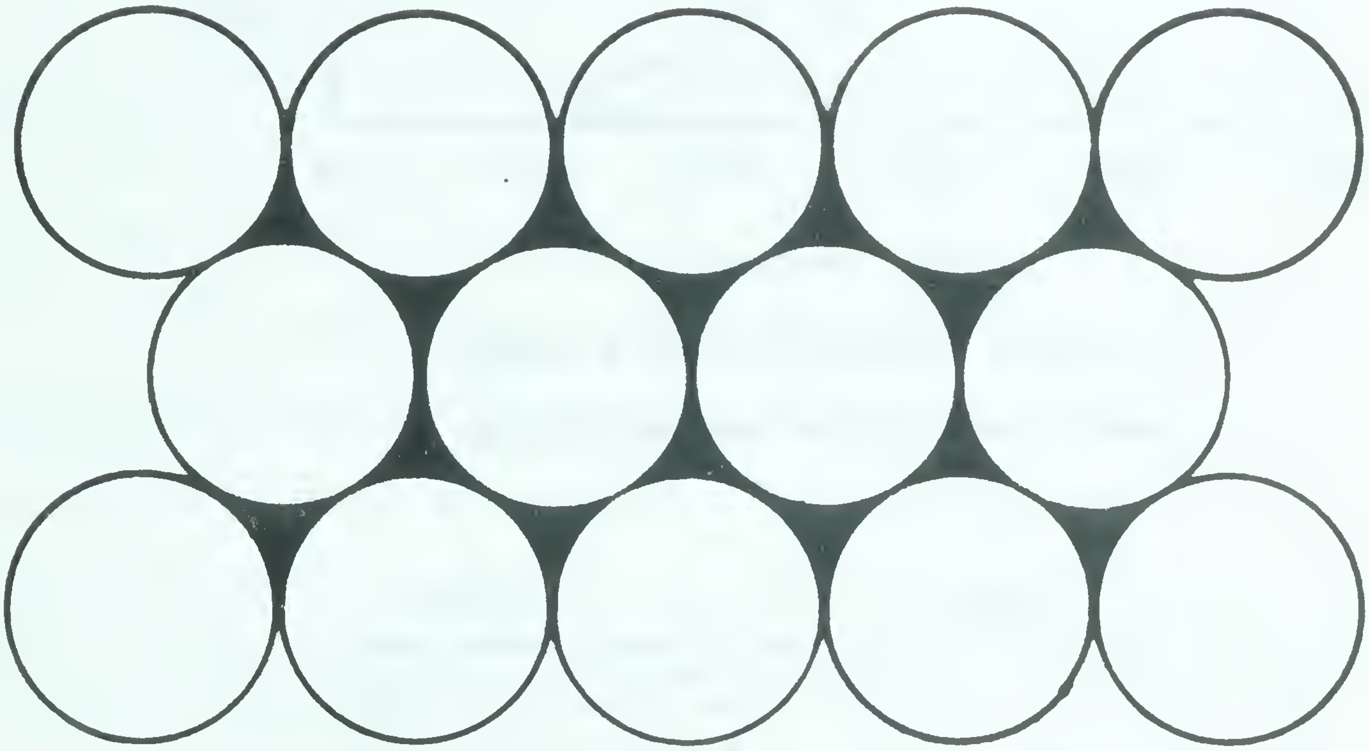

Fig. I Atomic Positions in a Close Packed Surface, the (111) Surface for a Face-Centered Cubic Crystal

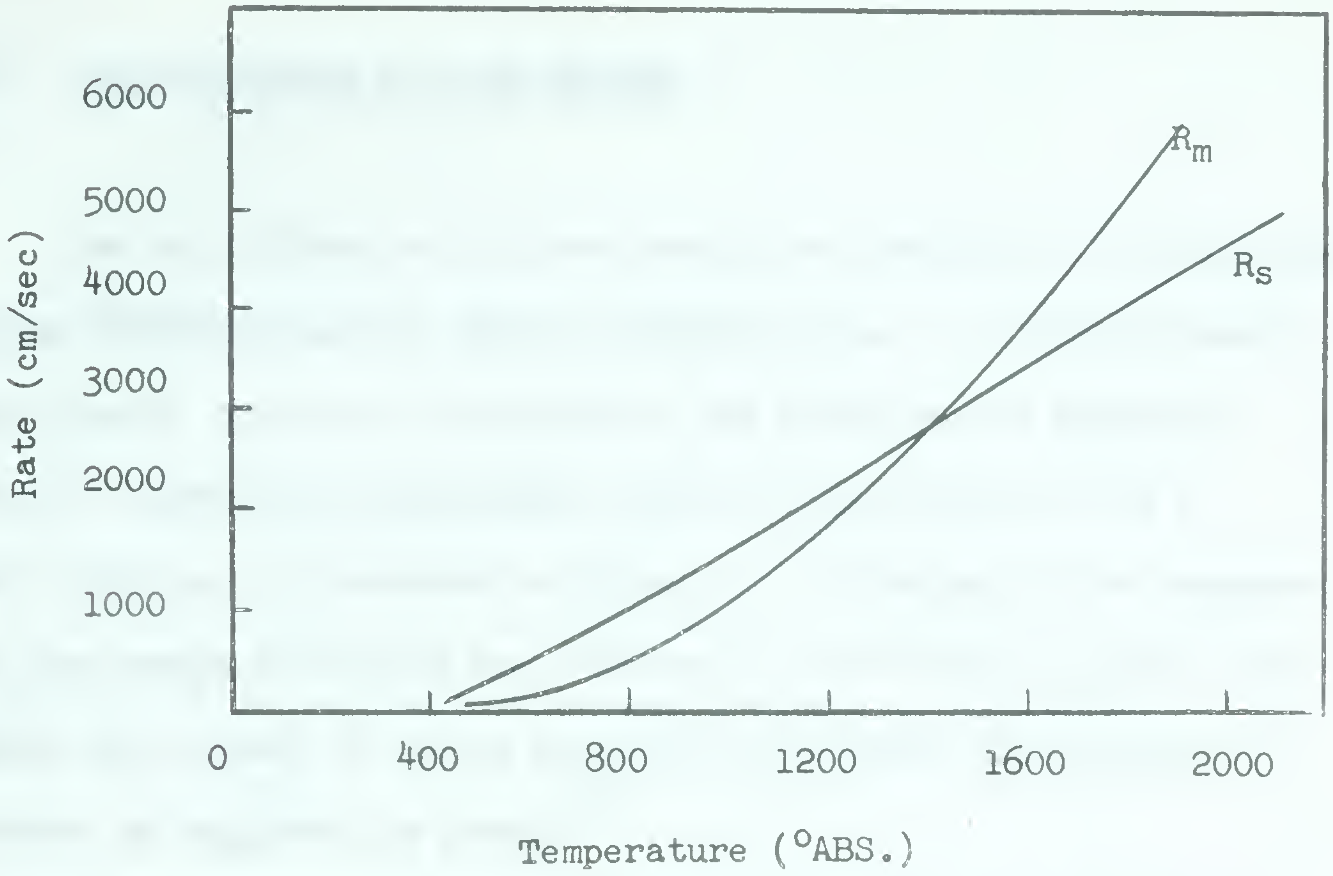

Figure 2. (After Chalmers[3]) Rates of solidifying and melting for copper.

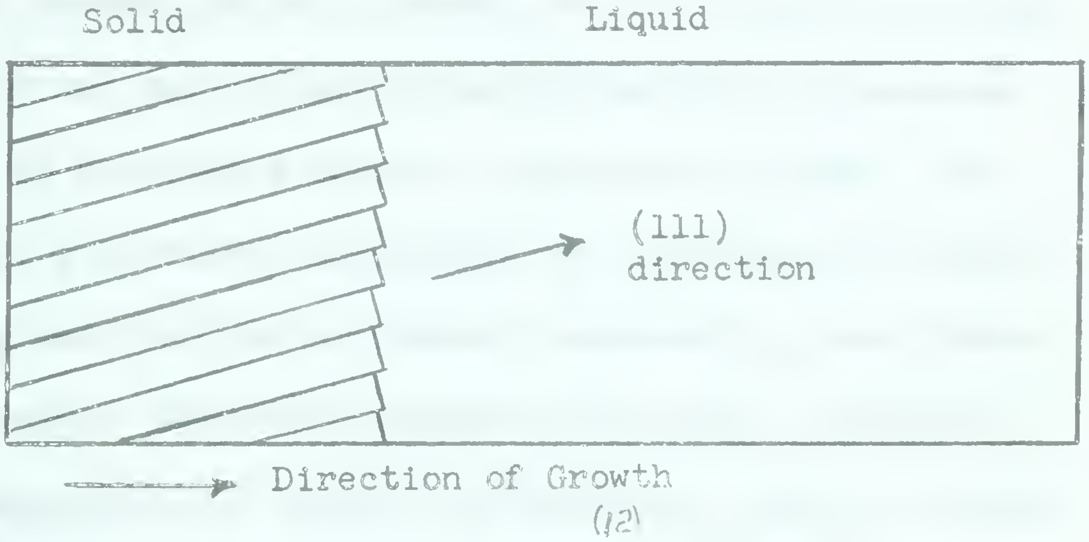

Figure 3. (After Winegard[12]) Schematic drawing of the surface of a crystal growing by the edgewise extension of close-packed planes.

B. SOLIDIFICATION OF PURE METALS

The solidification of pure metals may proceed by two different mechanisms depending on the rate of solidification. If solidification proceeds slowly, growth will proceed by the addition and edgewise extension of layers of close-packed planes which gives rise to a terraced structure illustrated in Figure 3. The edges of the terraces provide low energy sites for the addition of new atoms so growth need not depend upon layers of atoms spreading from screw dislocations at the surface as suggested by Frank(4).

If growth proceeds at a relatively fast rate, the liquid ahead of the interface will become thermally supercooled and dendritic growth will occur because a plane interface cannot dissipate the latent heat fast enough to satisfy existing conditions(9). Growth can occur much more rapidly if the latent heat of solidification is generated at a small tip and is dissipated into the surrounding liquid. Also, a "spike" (dendritic projection) generating out into the supercooled liquid is advancing into regions of greater supercooling, and, therefore, it advances faster than the remainder of the solid. Further, the latent heat generated by a "spike" will heat the liquid in nearby regions thereby preventing growth of other "spikes" nearby. Thus, there is a minimum separation of "spikes". Secondary "spikes" growing from primary "spikes" tend to form for the same reason that primary "spikes" form, because there are regions of supercooling in the vicinity of the primary "spike". Similarly, ternary and higher order "spikes"

are formed thus leading to the typical "pine tree" appearance characteristic of dendritic growth.

C. SOLIDIFICATION OF BINARY ALLOYS

1. Solute Distribution

In considering the solidification of binary alloys it is convenient to define a distribution coefficient, k_o, given by

$$k_o = \frac{C_S}{C_L} \qquad (5)$$

where C_S and C_L are the solute concentrations in the solid and liquid respectively at a given temperature (Figure 4). k_o may be either greater or less than unity depending upon the phase relationships of the system. For simplicity only values of k_o less than unity will be considered, but the theory is applicable to any value.

Consider an alloy of composition X. The first solid to form on solidification will be of composition $k_o X$ (Figure 5). This statement is true for all solidification rates providing local equilibrium exists. However, the microscopic picture of the solute distribution will be determined by the solidification rate.

(a) Very Slow Solidification

If solidification proceeds extremely slowly and there is sufficient time for complete diffusion in the solid, the solidified ingot will be of uniform composition for concentrations within the solid solubility limits.

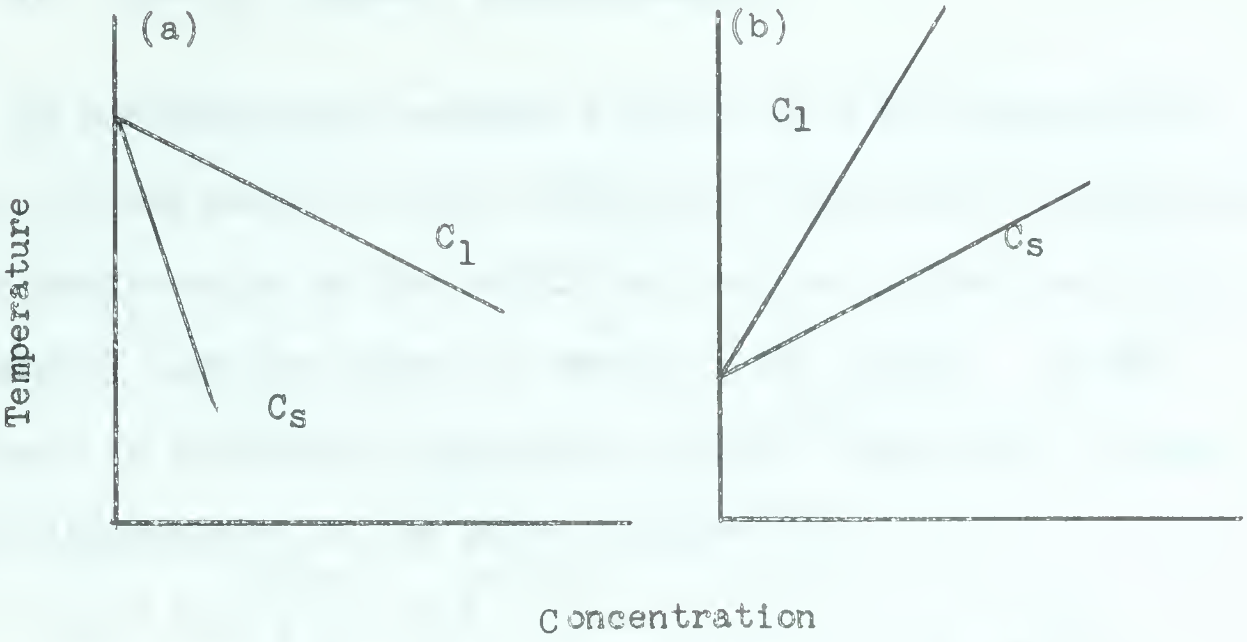

Figure 4. The distribution coefficient, $\frac{C_s}{Cl} = k_o$.

(a) $k_o < 1$ (b) $k_o > 1$

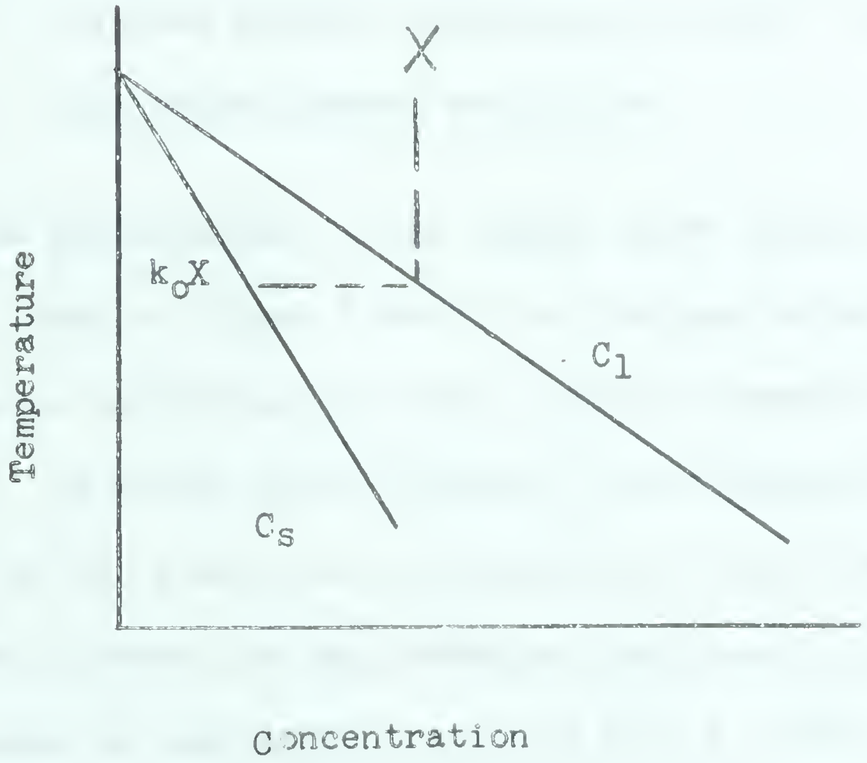

Figure 5. Solidification for $k_o < 1$.

[illegible]

[illegible]

[illegible]

[illegible]

(b) Slow or "Normal" Solidification

If solidification proceeds slowly, say a few centimeters per hour, but fast enough so that diffusion in the solid is negligible, the solute distribution in the solidified ingot will take one of two forms depending upon the amount of mixing in the liquid. If the entire liquid is of uniform composition, Phann(5) shows that the concentration distribution in the solid is given by:

$$C_s = k_o C_o (1-g)^{k_o - 1} \tag{6}$$

where:

C_s = concentration in the solid

k_o = distribution coefficient (assumed constant)

C_o = initial uniform composition of the liquid

g = fractional amount solidified

The solute distribution in the liquid under these conditions takes the form shown in Figure 6 and is a good approximation for the case of very slow solidification where liquid homogenization may be almost complete. In actual fact, however, liquid homogenization is not complete because of the finite solidification and slow diffusion rates. If the solute rejected at the interface continually piles up, it will diffuse away in the normal manner to give a liquid concentration curve similar to that shown in Figure 7. The mathematical expression for this concentration in the liquid, as derived by Smith et al(6) for the steady state is given by

$$C_\ell = C_o \left[1 + \left(\frac{1-k_o}{k_o} \right) e^{-(R/D)x'} \right] \tag{7}$$

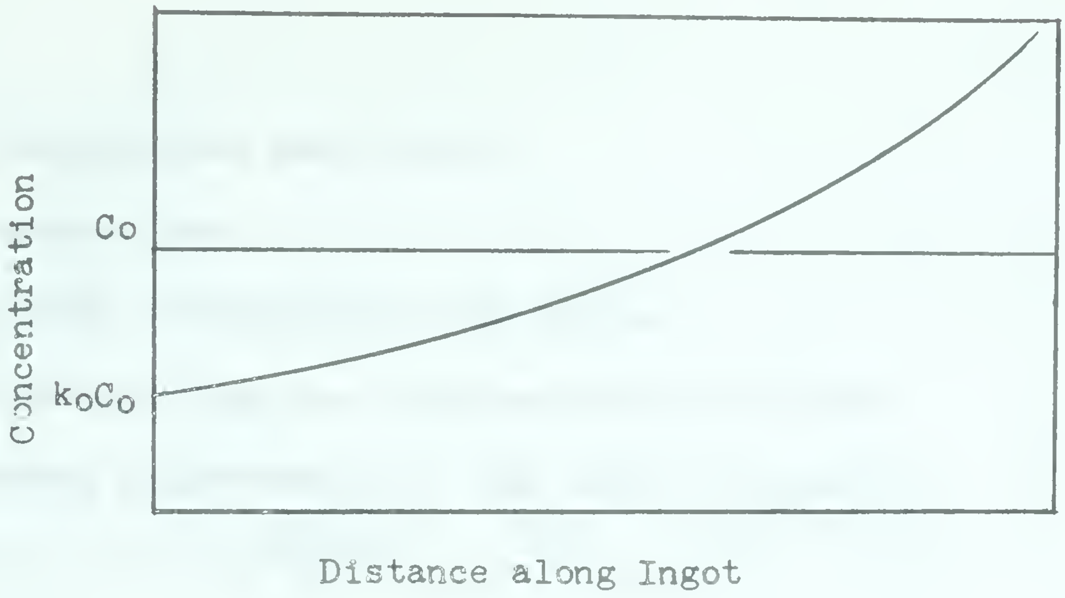

Figure 6. Solute distribution in the solid for the case of complete mixing in the liquid.

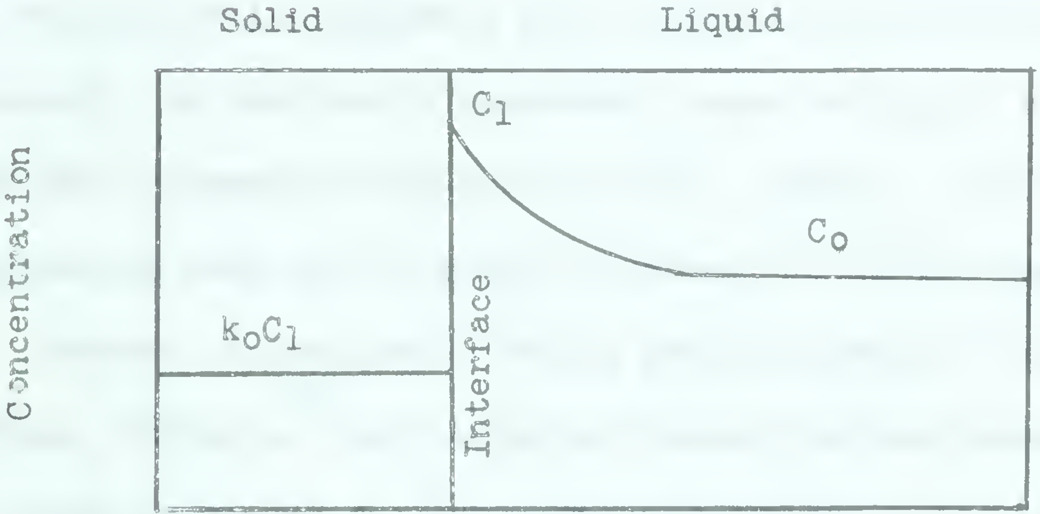

Figure 7. Concentration gradient in the liquid at the interface.

where

k_o = distribution coefficient

R = growth rate

D = liquid diffusivity of the solute

x' = distance from the interface into the liquid

The corresponding concentration in the solid is given by

$$C_S(x) = \frac{C_o}{2}\left\{1 + \mathrm{erf.}\left(\frac{\sqrt{(R/D)x}}{2}\right) + (2k_o - 1)e^{-k_o q (R/D)x} \cdot (\mathrm{erfc.})\left(\frac{2k_o-1}{2}\right)\sqrt{(R/D)x}\,\right)\right\} \qquad (8)$$

where

$q = 1 - k_o$

This solid distribution takes the form shown in Figure 8.

(c) Rapid Solidification

If solidification proceeds at a relatively fast rate, dendritic growth will occur. As previously suggested, supercooling is a prerequisite for the occurence of dendrite growth. However, in binary alloys, supercooling need not be solely "thermal" as is the case for pure metals. Because of the concentration gradient ahead of the solid - liquid interface, Chalmers (3) has suggested "constitutional supercooling" may occur as shown in Figure 9. T_e is the equilibrium solidification temperature and T_a is the actual temperature gradient which is controlled by the rate of heat withdrawal. $(T_e - T_a)$ at any point is, therefore, the amount of constitutional supercooling.

Under conditions of dendritic growth, inverse segregation will occur. The solute distribution in the primary ingots is still

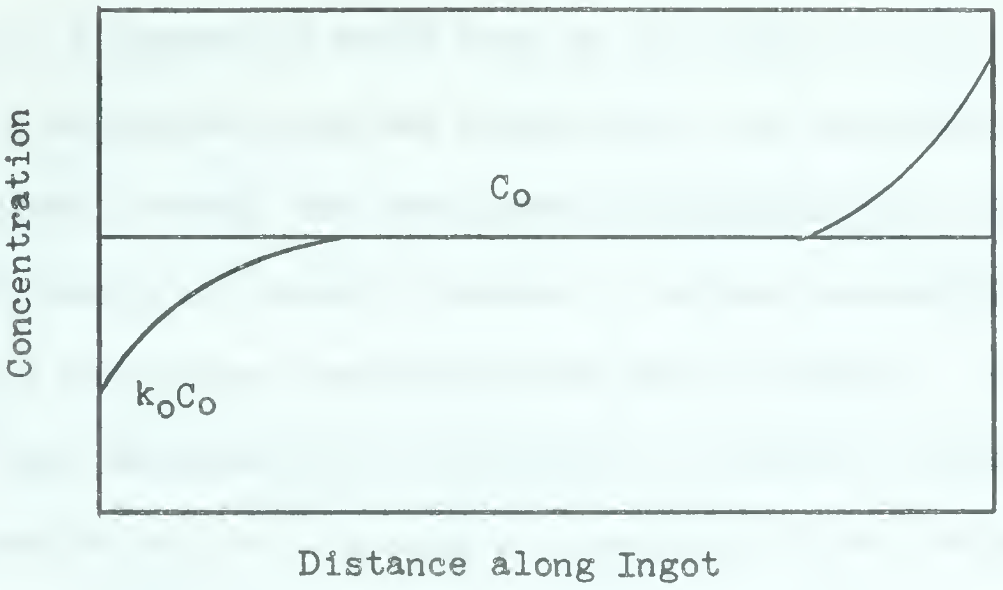

Figure 8. Solute distribution in the solid for slow solidification when transport in the liquid is by diffusion only.

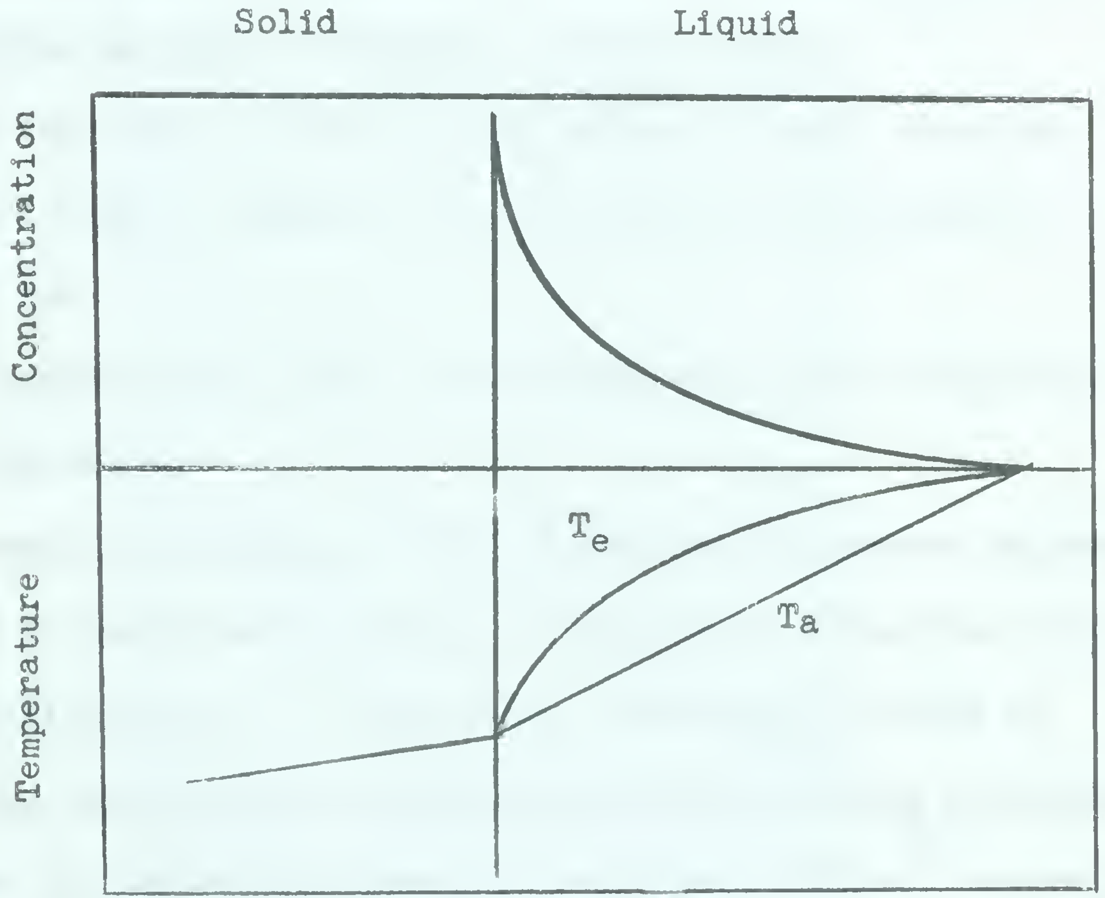

Figure 9. (After Chalmers(3))
Constitutional supercooling ahead of an advancing solid - liquid interface.

in the order of $k_o X$ (Figure 5) while that of the liquid is $\frac{X}{k_o}$, but as the dendrites are solidifying and contracting, the enriched residual liquid is drawn back through the interdendritic channels into the contraction cavities causing an overall increase in solute concentration in the region of the ingot where solidification was initiated. Kirkaldy and Youdelis(2) have mathematically formulated the inverse segregation mechanism and have shown that the solute distribution for inverse segregation takes a form similar to that shown in Figure 10.

The underlying assumptions of inverse segregation theory are:

(1) there is complete flowback of residual liquid during the solidification so that no shrinkage porosity occurs,

(2) local equilibrium exists at the solid - liquid interface,

(3) solid coring is complete, i.e., there is no diffusion in the solid, and

(4) the interdendritic liquid is homogeneous at any particular level of the ingot.

It should be pointed out that the theory of inverse segregation, as developed by Kirkaldy and Youdelis, is applicable to systems which expand upon solidification. In this case, the enriched liquid is forced out of the interdendritic channels and the resulting segregation is not "inverse" in the general sense of the term. Colton(1) has shown that the theoretical segregation, based upon the theory of inverse segregation, in bismuth(rich)- antimony alloys which expand upon solidification, is in good agreement with the experimental segregation.

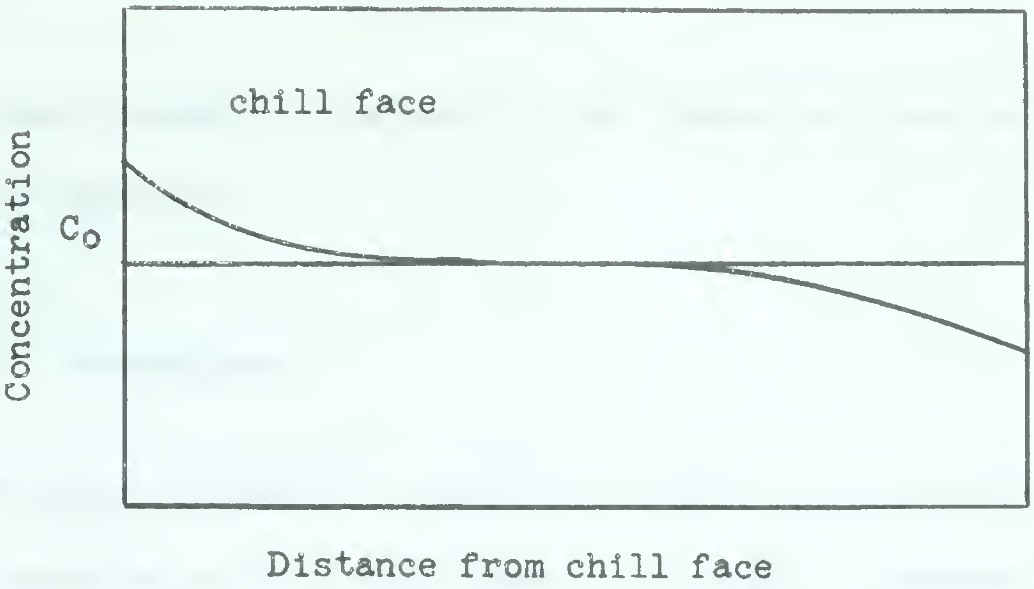

Figure 10. Solute distribution for inverse segregation.

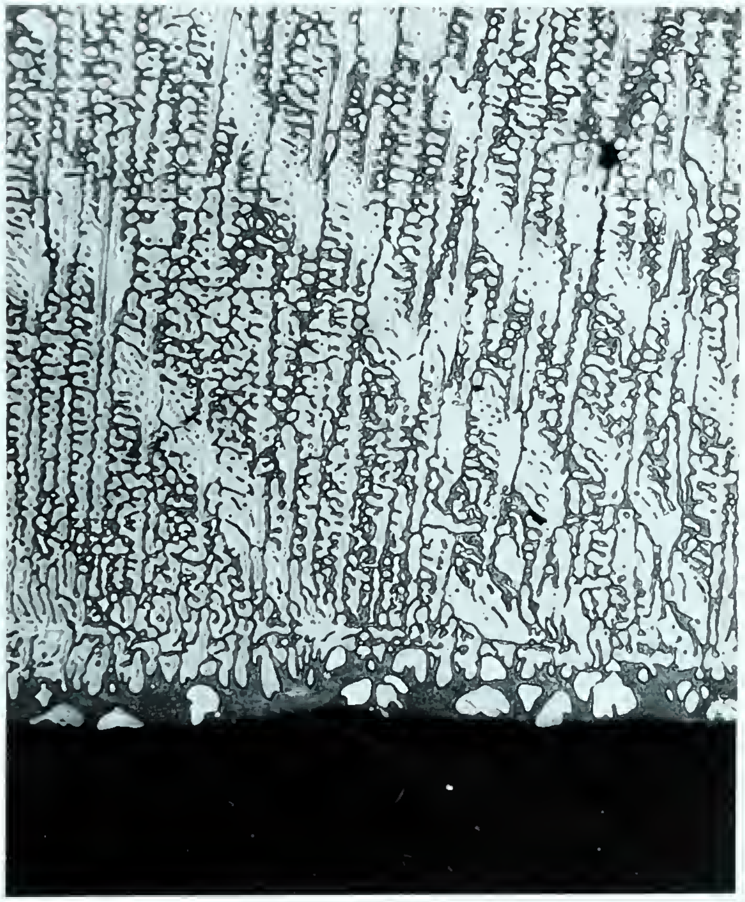

Figure 11. Massive exudations caused by remelting.

A more complete treatment of the theory of inverse segregation appears in the appendix.

(d) Exudations

The term "exudation" refers to a layer of low-melting-point constituent occuring at the chill face of an ingot. "Massive exudations", shown in Figure 11, are a result of remelting of the low-melting-point constituent and the ensuing drawback of the constituent to the surface of the ingot. Even in the absence of remelting, surface tension forces may be sufficient to draw a thin layer of constituent to the surface of the ingot if a decrease in interfacial energies is involved. The latter type of exudations is shown in Figure 12.

Exudations are not part of the mechanism of "inverse" segregation", so in the determination of inverse segregation, a correction must be made by the extrapolation of points near the chill face which are not affected by the exudations.

2. Macrostructure of Binary Alloys

The macrostructure of a solidified ingot is dependent upon the temperature and concentration distributions during solidification. If the rate of solidification is slow, the concentration and temperature gradients in front of the interface will not be large, and a plane interface will result. However, if "constitutional supercooling"

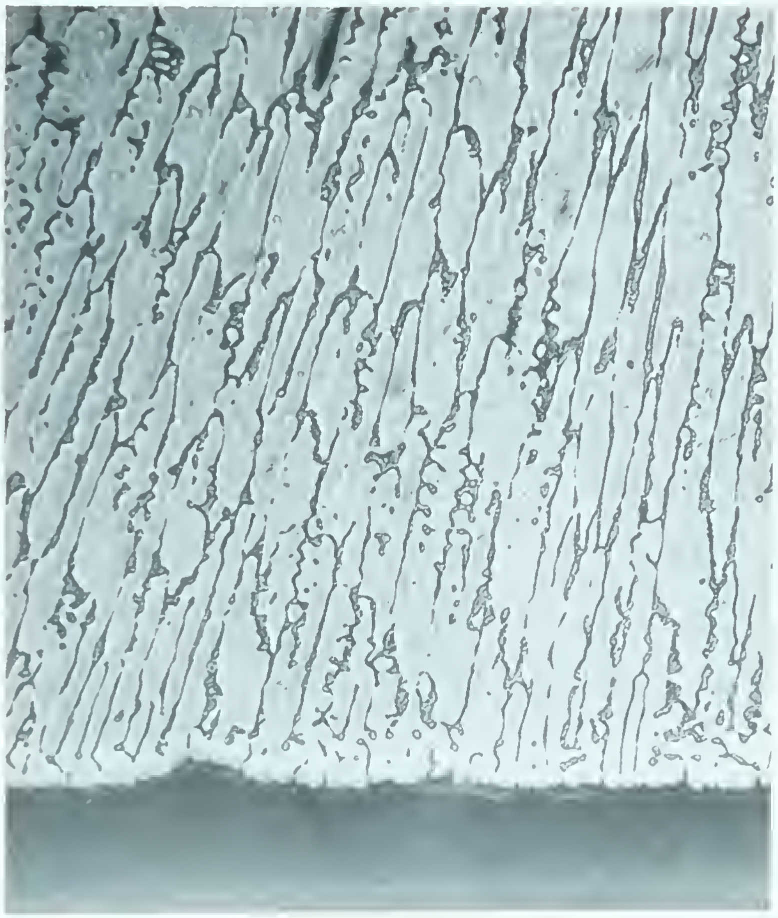

Figure 12. Exudations caused by surface tension forces (X100).

exists to a small extent dendritic projections will extend out a short distance into the liquid. These projections tend to form a cellular structure which has been oberved.(7) Tiller and Rutter (7) predicted that the transition from a plane interface to a cellular one occurs at a certain critical ratio of temperature gradient, G, to growth rate, R, as follows:

$$\frac{G}{R} = -m'C_0(1-k_0)/Dk_0 \qquad (9)$$

where m' is the slope of the liquidus line, C_0, is the initial concentration in the melt, D is liquid diffusion coefficient of the solute, and k_0 is the distribution coefficient. The onset of cellular growth was found to conform very accurately to the predicted results.

As the rate of solidification of the alloy is increased, the amount of "constitutional supercooling" is usually found to increase, resulting in a transition from cellular to dendritic growth. Tiller and Rutter (7) have found that the transition from cellular to dendritic growth occurs at a critical ratio of temperature gradient in the liquid, G, to the square root of the growth rate, $R^{1/2}$, as follows:

$$\frac{G}{R^{1/2}} = AC_0 \qquad (10)$$

where A is a proportionality constant.

If constitutional supercooling becomes very great, nucleation will occur ahead of the advancing solid - liquid interface resulting in an equiaxial structure. The high degree of supercooling results from the gradual decrease in the steepness of the temperature gradient

as the solid - liquid interface advances away from the chill face of the ingot, while the concentration gradients do not decrease nearly so rapidly because of the slow diffusion rate.

III EXPERIMENTAL

A. Apparatus

1. The Magnets

The field parallel to the direction of solidification was supplied by a water-cooled solenoid (see Figure 13) adapted from the design of Daniels(8). (Details of the construction are given by Colton(1).) The solenoid provided a maximum field of 16,000 oersteds uniform to ± 5% over a cylindrical volume 3" long and 1" in diameter.

The field perpendicular to the direction of solidification was obtained using a water-cooled, pole-type electromagnet which was an adaptation of the Uppsala Electromagnet(10). The pole-type magnet, (Figure 14) supplied a maximum field of 35,000 oersteds uniform to ± 3% over a cylindrical volume 3½" in diameter and 1½" in length.

Power was supplied to the magnets by a thirty-six kilowatt, direct current, constant voltage generator, which gave a maximum voltage of 48 volts with a ripple of ± 2%.

2. Casting Unit

The casting unit, comprising a resistance furnace, a graphite mold, and a water jet is shown schematically in Figure 15. The mold approximately 3" long and 7/8" in diameter was tapered inside for easy removal of the solidified ingot. A hole, ½" in diameter was drilled through the side and near the top of the mold to admit the

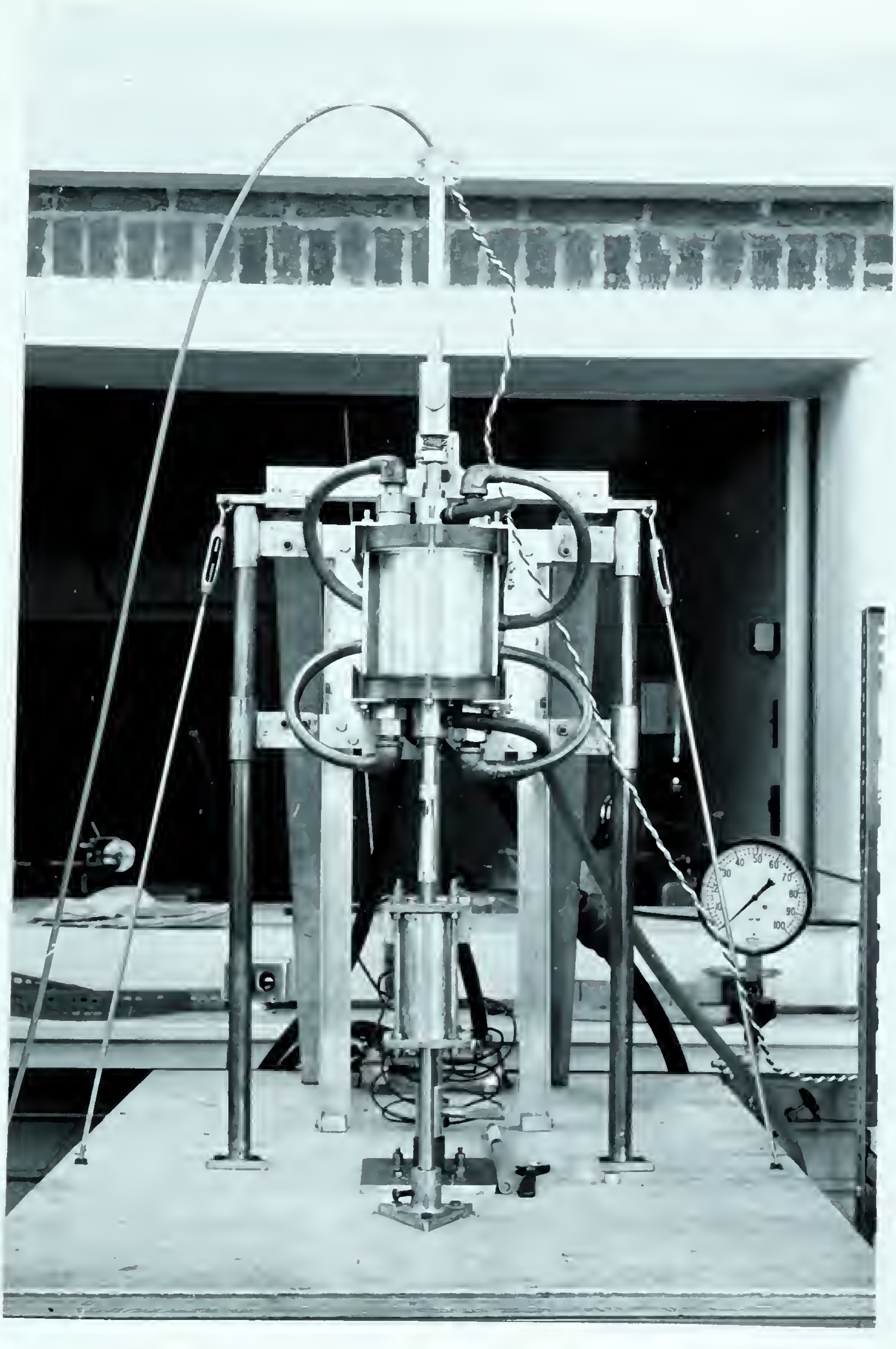

Figure 13. Solenoid Magnet and Solidification Apparatus .

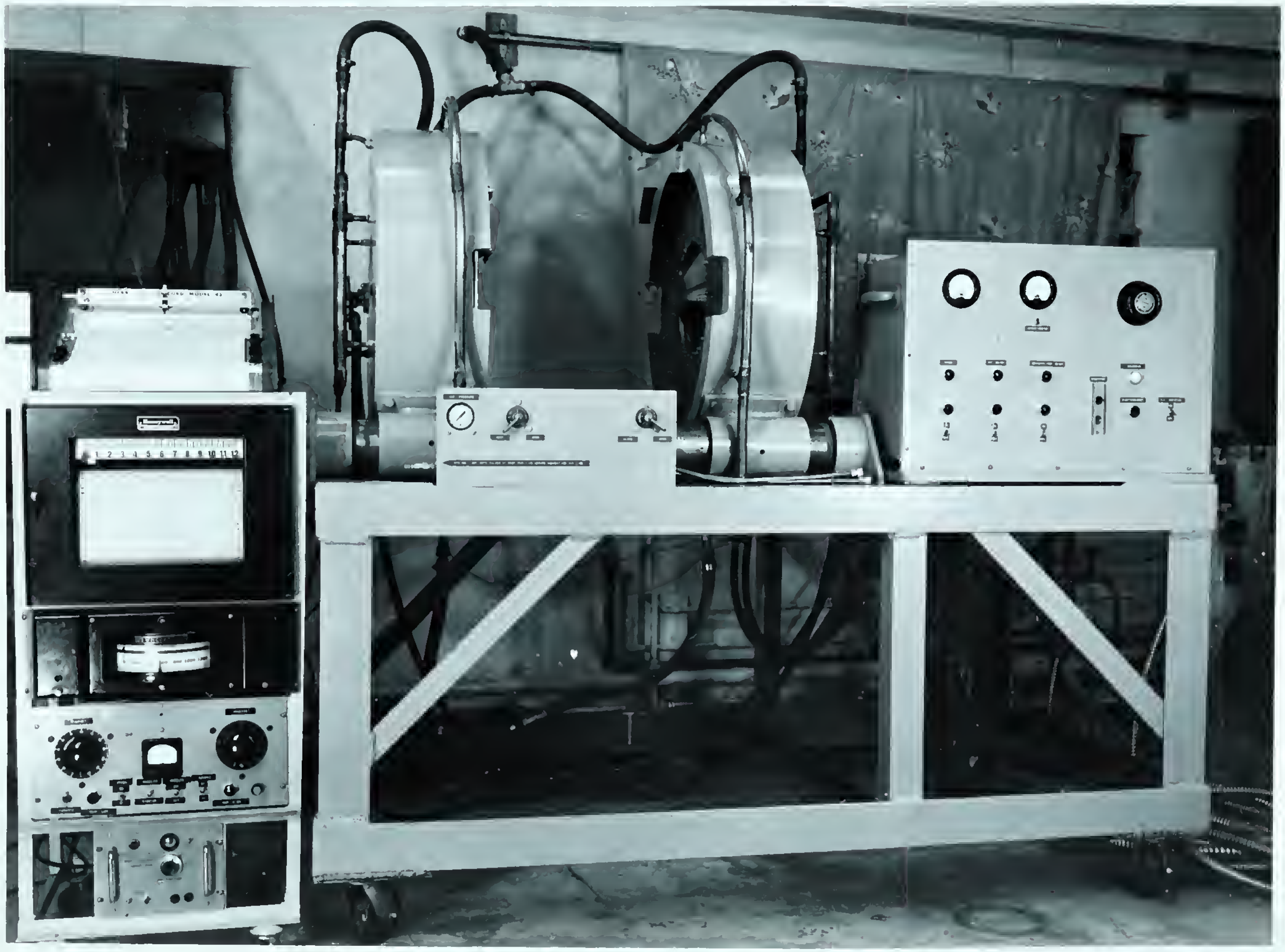

Figure 14. Pole-Type Electromagnet.

molten alloy. The mold was clamped between lengths of stainless steel tubing, the bottom support housing a length of $\frac{1}{4}$" brass tubing which impinged water on the baseplate to ensure unidirectional solidification.

A 28 gauge, chromel - alumel thermocouple and a length of 1/8" stainless tubing for degassing purposes were placed in the mold as shown in Figure 15. The thermocouple, 1/8" tubing and the baseplate were coated with an alundum slurry to protect them from attack by the molten metal.

B. METHOD

Four hundred grams of master alloy containing 10% copper were prepared from aluminum (99.91%) and electrolytic copper (99.96%). Portions weighing about 40 gms. were then remelted in a graphite crucible, bubbled vigorously with argon to remove dissolved gas and to ensure homogenity, and were then poured into the mold which was heated to over 700°C. The alloy was held at this temperature and again bubbled vigorously with argon to remove any gas picked up during the pouring operation. The bubbling tube was removed from the melt and the ingot was lowered into the field. (When the solenoid was used, the solenoid was lowered around the ingot.) The temperature was allowed to drop until 50°C of superheat remained at which time the thermocouple was removed from the molten alloy and solidification started by impinging water on the baseplate. After the ingot was completely solidified it was removed from the mold, and the degree of segregation was determined by a volumetric analysis.

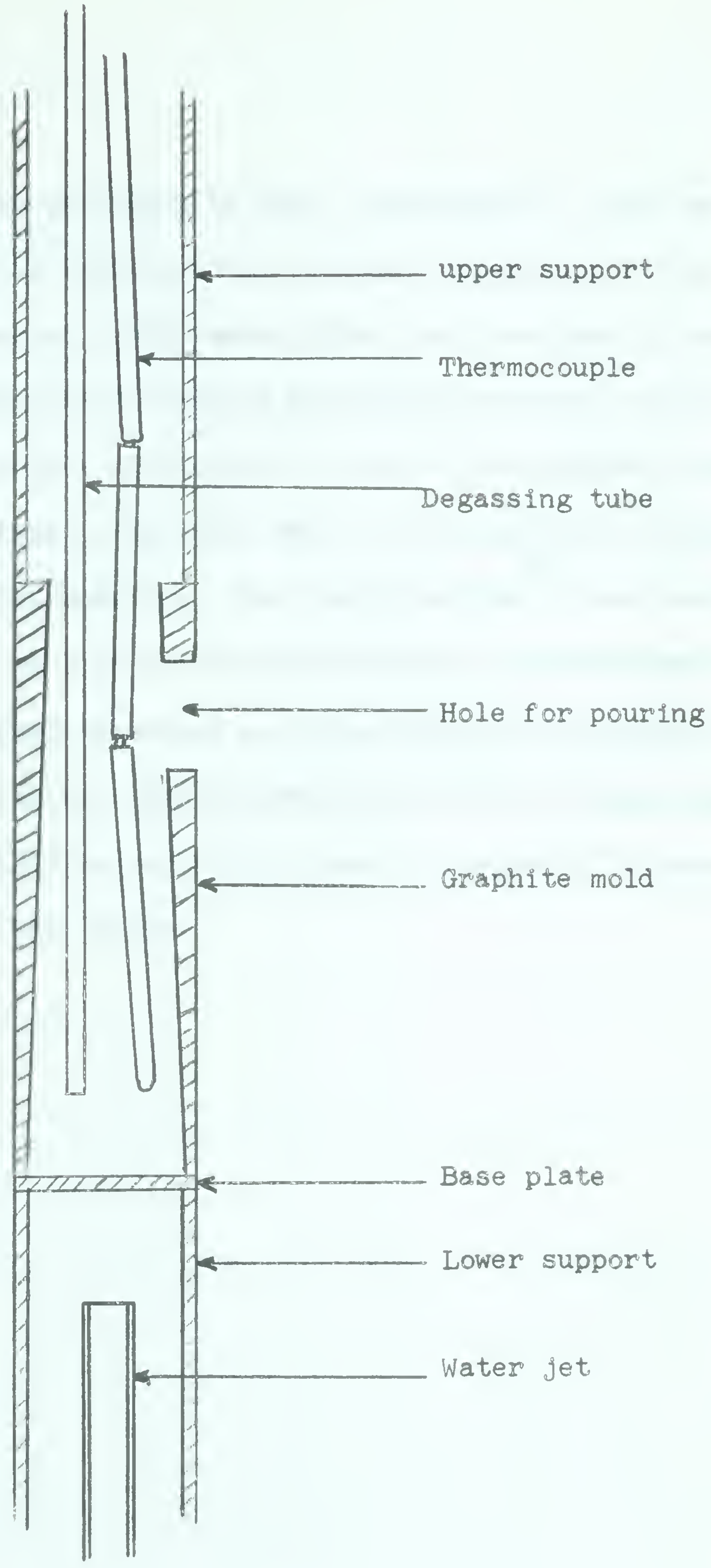

Figure 15. Schematic diagram of casting unit .

C. ANALYSIS

The ingots were sawn in half longitudinally and the cuttings collected in order to determine the average composition of the ingot. Five successive cuts of 0.010" were milled from the base of one of the half sections and were analyzed for copper content. The results were extrapolated to the chill face to correct for surface exudations and finite sample size. The other half of the ingot was retained for metallographic examination. The iodide method (11) was used for determining copper content and all precautions of good volumetric analysis were followed to ensure good precision in the analysis between average and base samples. The standard deviation of average samples was found to be 0.025% copper which gives the degree of segregation an accuracy of ± 0.05% copper.

IV. RESULTS

A. METALLOGRAPHIC

The macrostructures of three typical aluminum - 10% copper ingots representing solidification in zero field, 13,000 oersteds applied parallel to the direction of solidification, and 34,000 oersteds applied perpendicular to the direction of solidification are shown in Figures 16 to 18. The dendritic growth patterns at the chill faces of the same three ingots are shown in Figures 19 to 21.

The macrostructures of the aluminum - 20% copper and aluminum - 5% copper ingots are shown in Figures 22 and 23; the dendritic patterns and exudations at the chill faces are shown in Figures 24 and 25.

B. SEGREGATION

Table #1 gives a comparison of the pertinent data for the ingots used in this investigation.

The maximum segregation occuring at the chill face for aluminum - copper ingots ranging from 0 to 33% copper solidified in field strengths of 13,000 oersteds applied parallel to the direction of solidification and 34,000 oersteds applied perpendicular to the direction of solidification are compared with no-field results in Figure 26.

Figure 16. Macrostructure of an Al - 10% Cu ingot cast in zero field (XI).

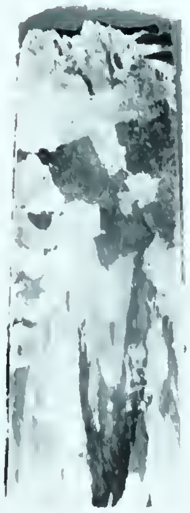

Figure 17. Macrostructure of an Al - 10% Cu ingot cast in a field of 13,000 oersteds applied parallel to the direction of solidification (XI).

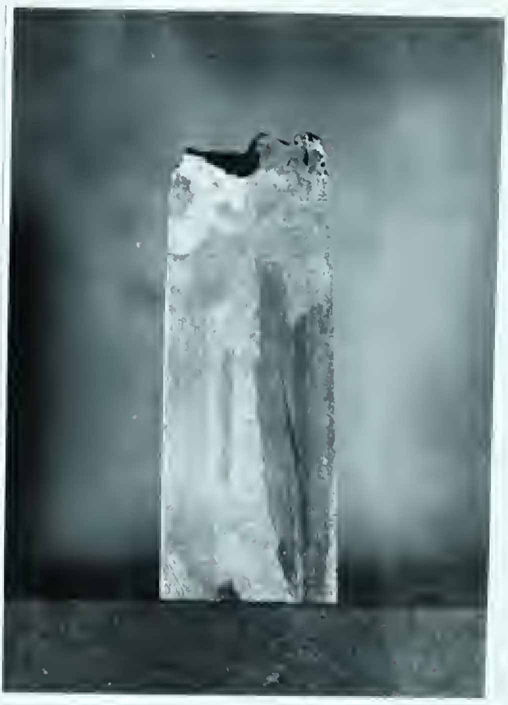

Figure 18. Macrostructure of an Al - 10% ingot cast in a field of 34,000 oersteds applied perpendicular to the direction of solidification (XI)

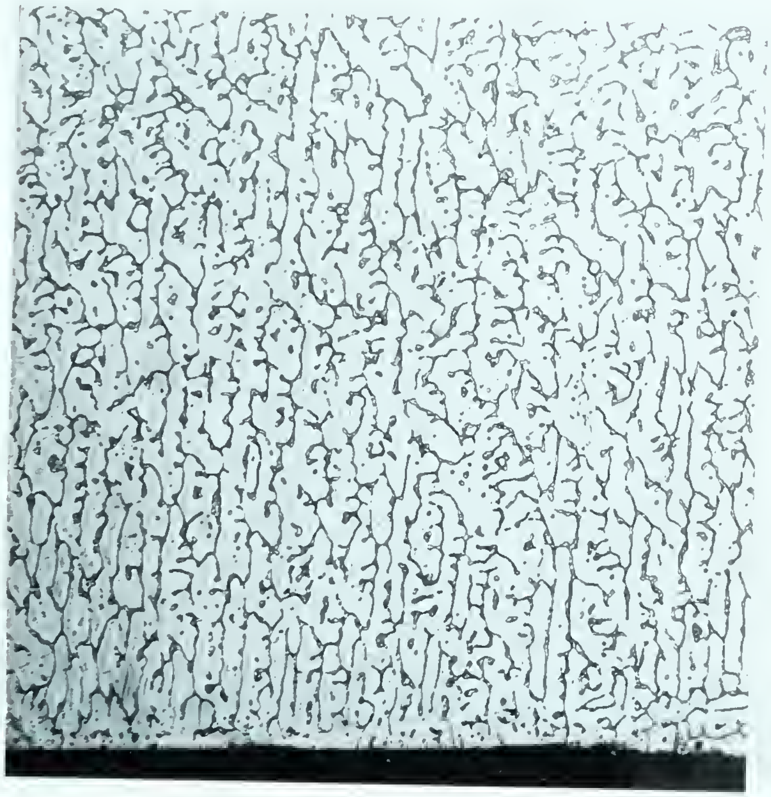

Figure 19. Microstructure of Al - 10% Cu ingot cast in zero field (X100).

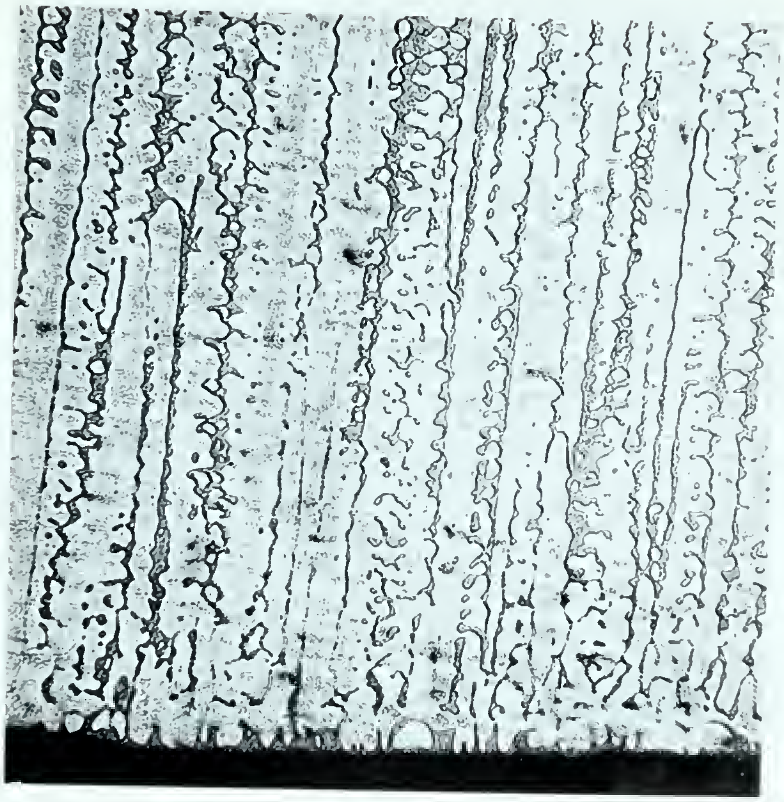

Figure 20. Microstructure of Al - 10% Cu ingot solidified in a parallel field of 13,000 oersteds (X100)

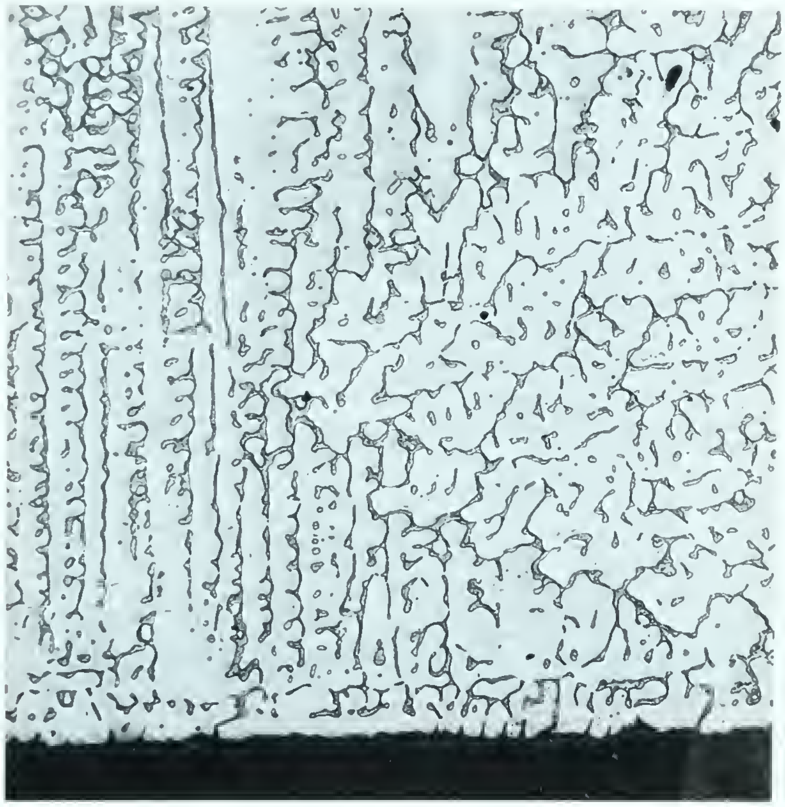

Figure 21. Microstructure of Al - 10% Cu ingot solidified in a perpendicular field of 34,000 oersteds (X100)

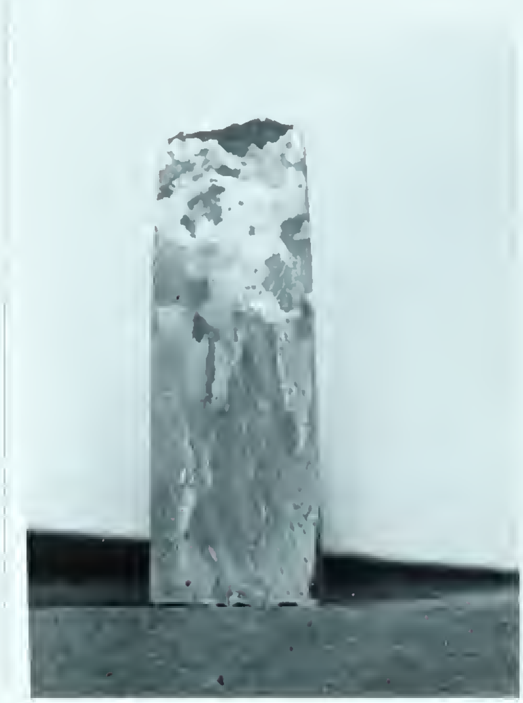

Figure 22. Macrostructure of Al - 20% Cu ingot solidified in a perpendicular field of 34,000 oersteds (XI).

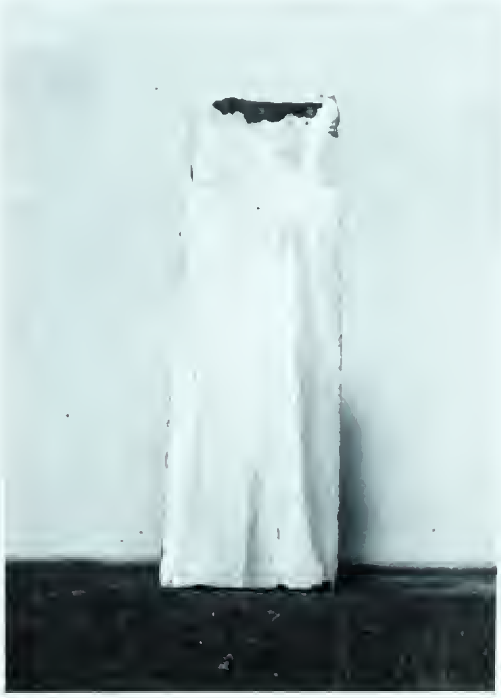

Figure 23. Macrostructure of Al - 5% Cu ingot solidified in a perpendicular field of 34,000 oersteds (XI).

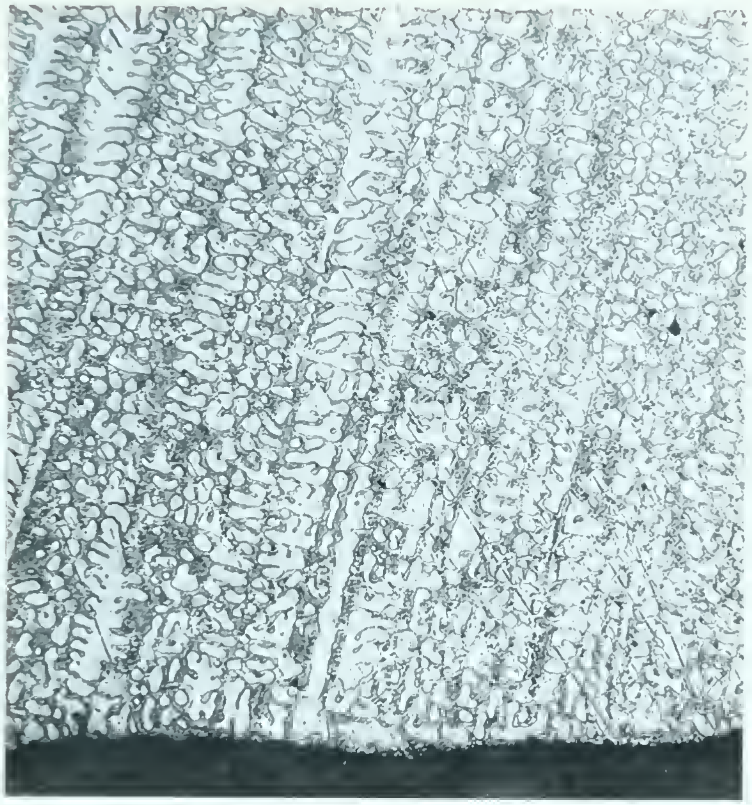

Figure 24. Microstructure of Al - 20% Cu ingot solidified in a perpendicular field of 34,000 oersteds (X100).

Figure 25. Microstructure of Al - 5% Cu ingot solidified in a perpendicular field of 34,000 oersteds (X100).

TABLE #1 Analysis of Ingots.

Ingot	Field Direction	Field Strength Oersteds	Average Composition % Cu	Base Analysis (% Cu) Position (Distance from Chill Face)						Maximum Segregation
				.005	.015	.025	.035	.045	Others	
8 - 0	-	0	16.20	18.95	16.50	16.25			0.2" 16.28	.51
14	parallel	13,000	10.36	11.12	10.98	10.93	10.79	10.84		.70
16	perpendicular	34,000	9.27	10.25	9.83	9.72	9.77	9.71		.80
17	perpendicular	10,000	9.29	10.14	9.55	9.73	9.58			.75
18	perpendicular	20,000	9.37	10.08	9.84	9.82	9.71	9.73		.77
19	perpendicular	5,000	9.29	9.85	9.85	9.75	9.71	9.79		.62
20	perpendicular	34,000	19.04	20.28	19.73	19.68	19.55	19.64		.80
21	perpendicular	34,000	4.51	5.26	4.85	4.70	4.73	4.53		.65
2	parallel	13,000	26.34	26.92	27.02	26.44	26.40	26.60		.38
3	parallel	13,000	20.52	21.80	20.91	20.83	21.06			.59
4	parallel	13,000	6.42	8.42	7.02	6.79				.60
11	perpendicular	13,000	9.84	10.55	10.50	10.44	10.41			.73
22	-	0	9.67	9.79	9.95	9.98	9.88	9.82		.50

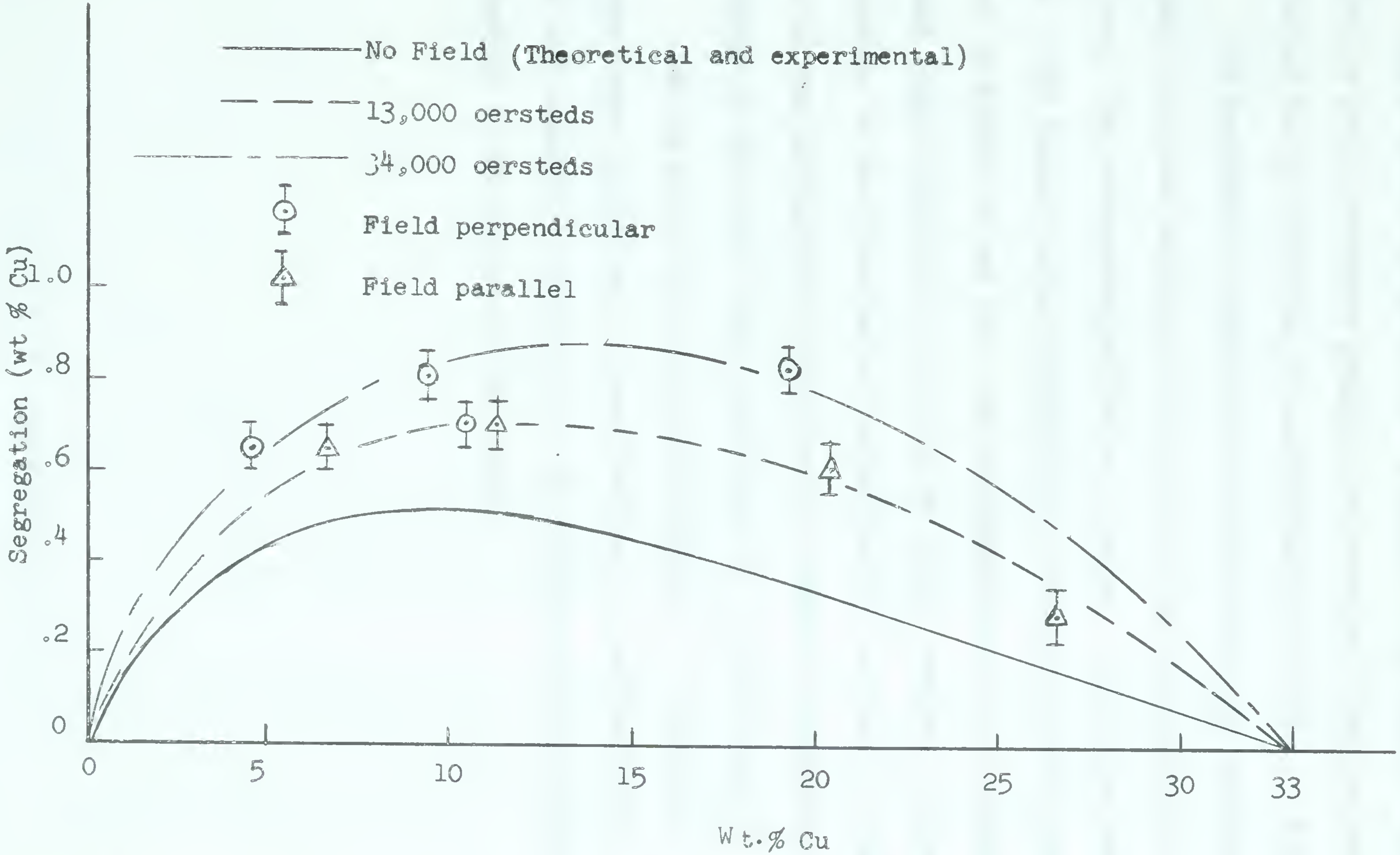

Figure 26. Maximum segregation in the Al - Cu System for field strengths of 13,000 and 34,000 oersteds.

The maximum segregation for aluminum - 10% copper alloys solidified in field strengths ranging from zero to 34,000 oersteds applied perpendicular to the direction of solidification is shown in Figure 27.

All segregation results were obtained from the extrapolation of at least four base samples, which corrects for exudations and finite sample size. The extrapolations for the aluminum - 10% copper and aluminum - 20% copper ingots solidified in a field of 34,000 oersteds are shown in Figure 28 and 29. The extrapolations for an aluminum - 10% copper ingot solidified in a field of 13,000 oersteds applied perpendicular to the direction of solidification is shown in Figure 30. The form of the extrapolation suggests the absence of exudations and a micrograph of the chill face (see Figure 31) verifies this.

Cooling curves for the solidification of an aluminum - 10% copper ingot solidified in zero field and a field of 34,000 oersteds are compared in Figure 32. The thermocouple was placed approximately in the centre of the ingot.

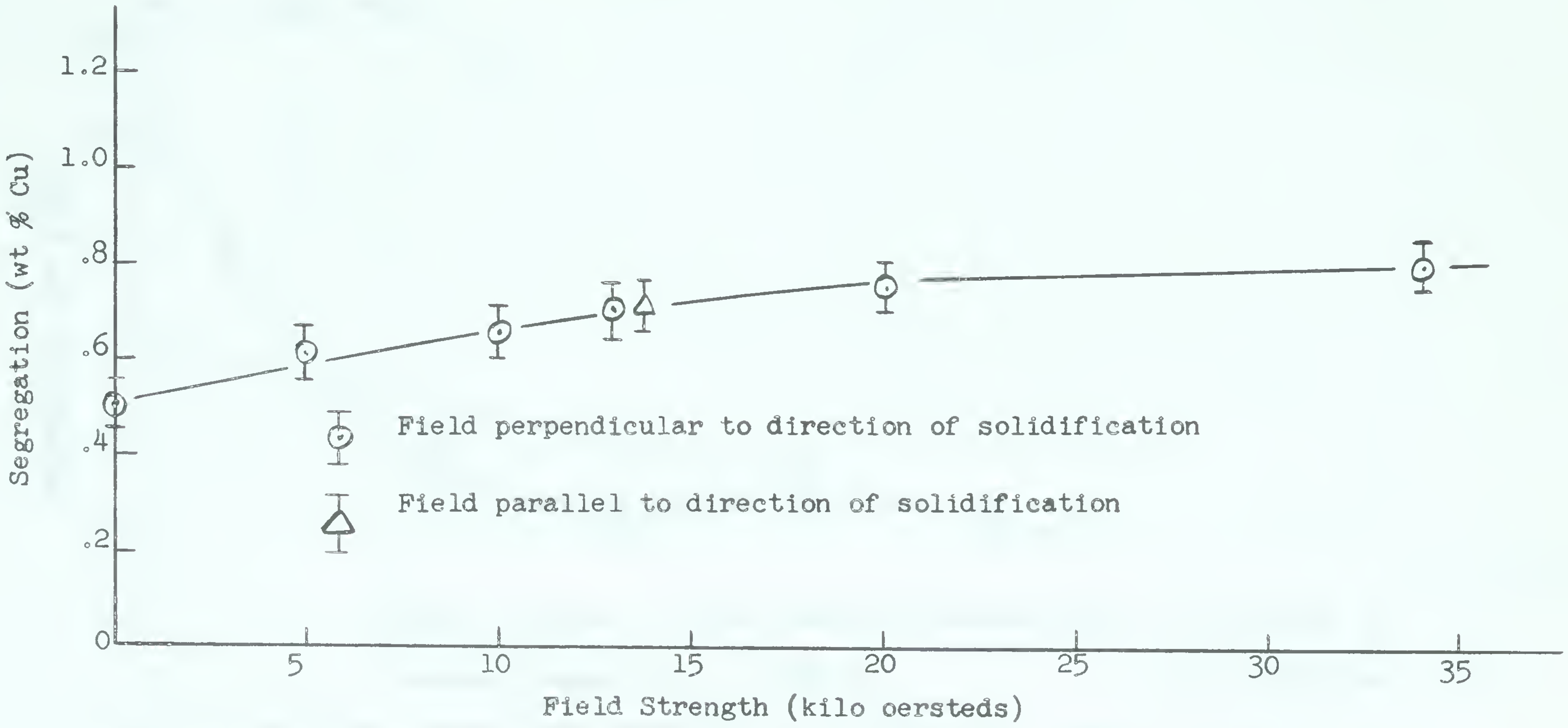

Figure 27. Effect of field strength on maximum segregation in Al - 10% Cu ingots .

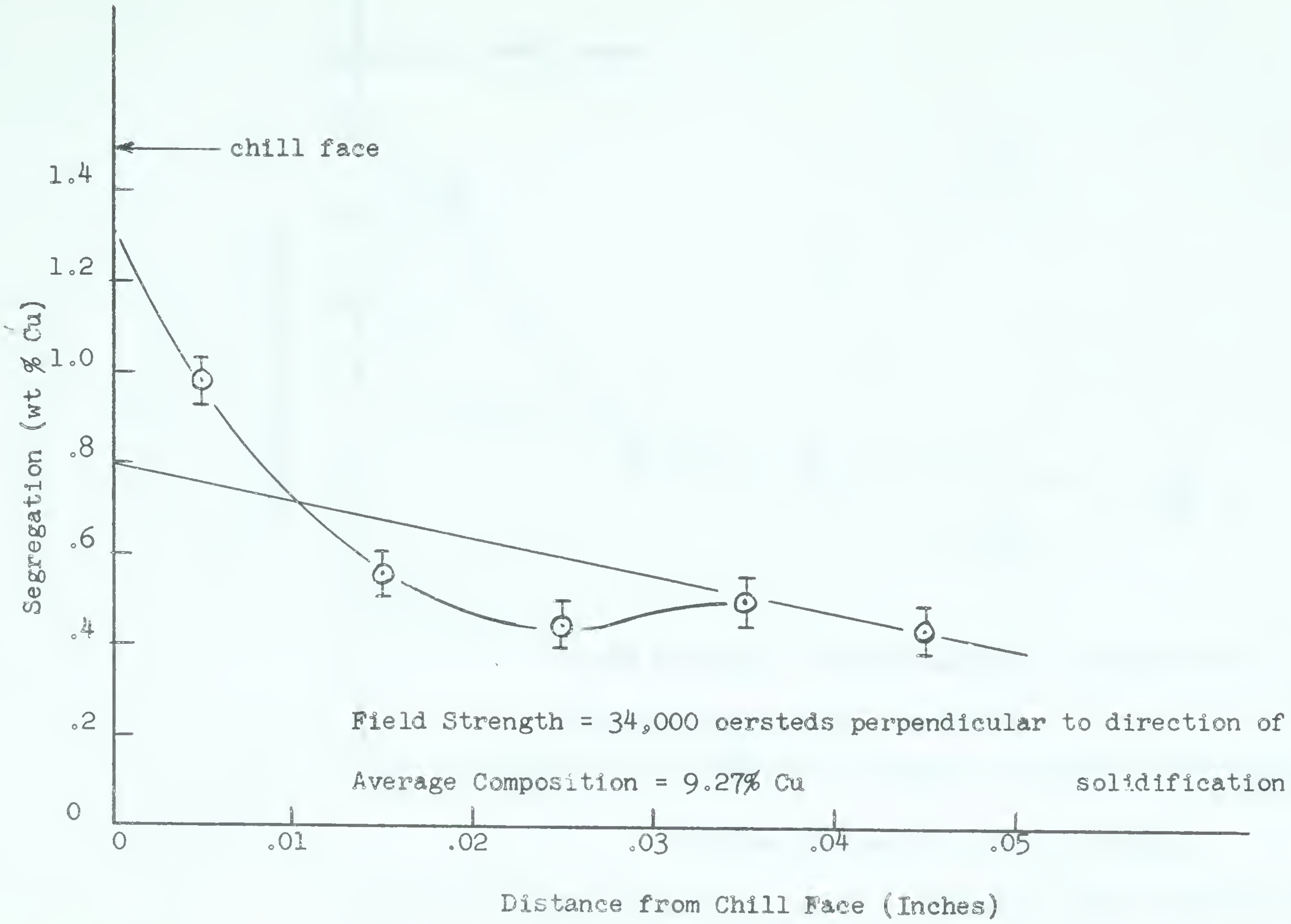

Field Strength = 34,000 oersteds perpendicular to direction of solidification

Average Composition = 9.27% Cu

Figure 28. Base Analysis of an Al - 9.27% Cu ingot showing the extrapolation correcting for exudations and finite sample size.

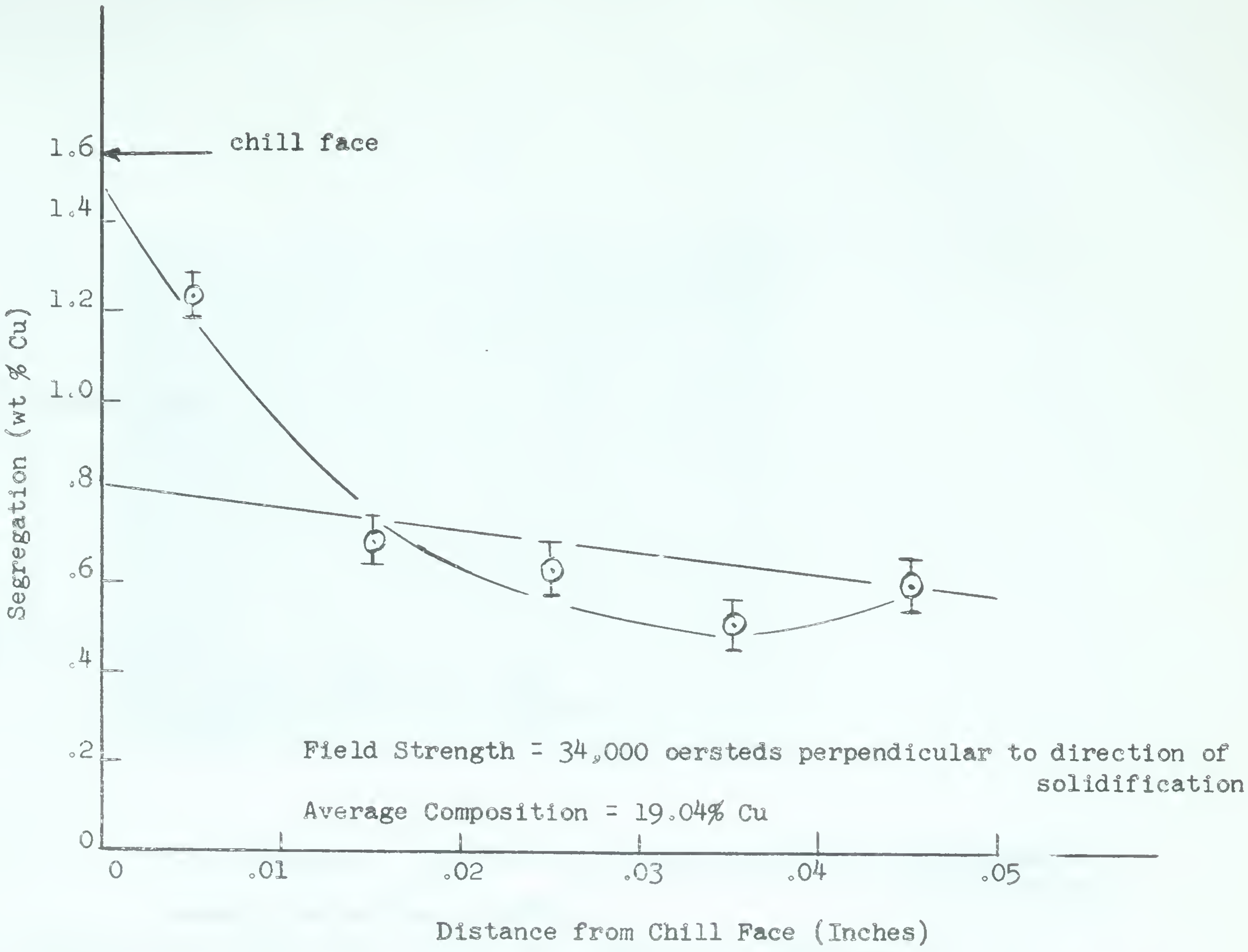

Figure 29. Base Analysis of an Al - 19.04% Cu ingot showing extrapolation correcting for exudations and finite sample size.

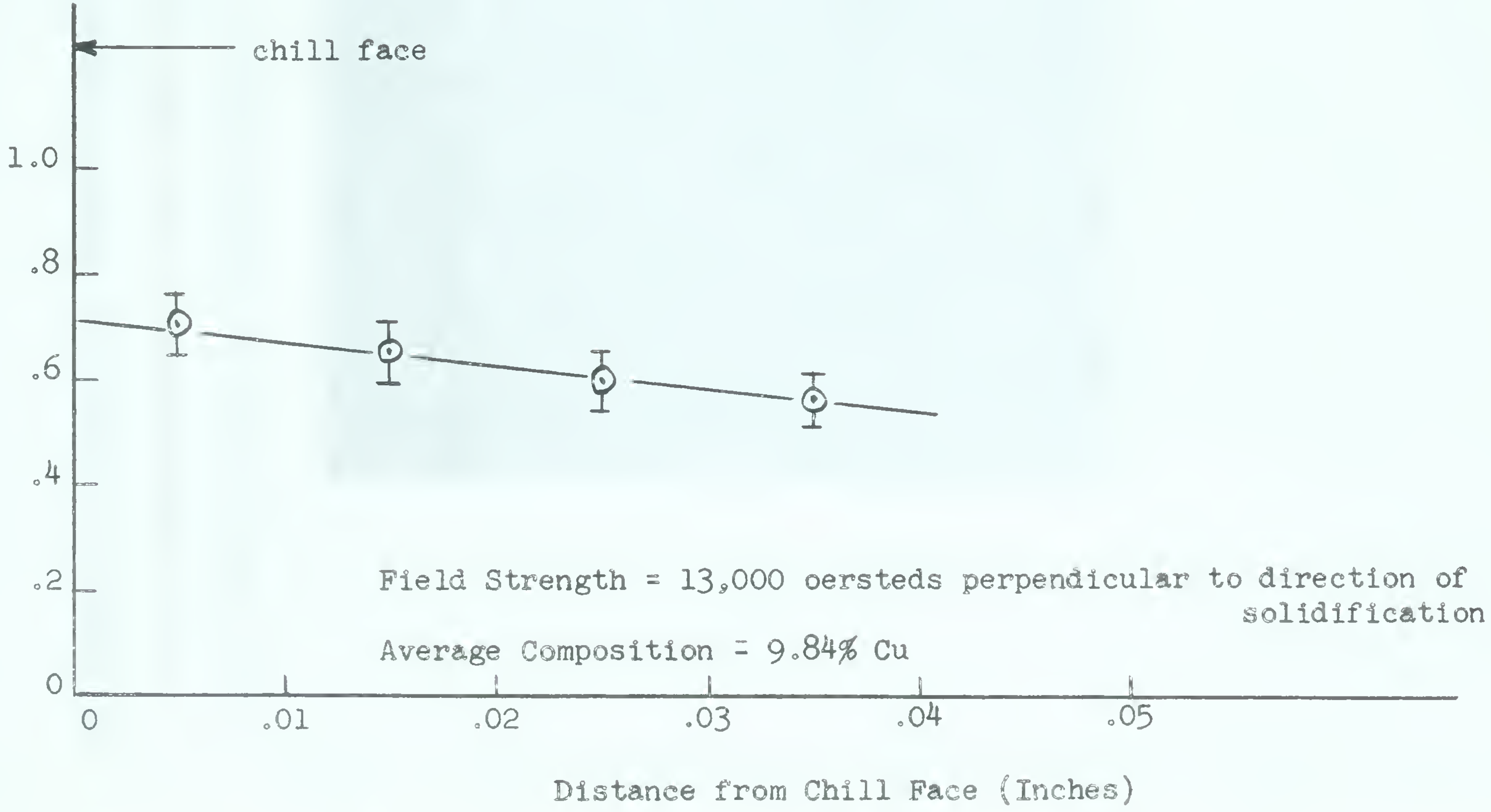

Figure 30. Base analysis of an ingot which had no exudations.

[illegible]

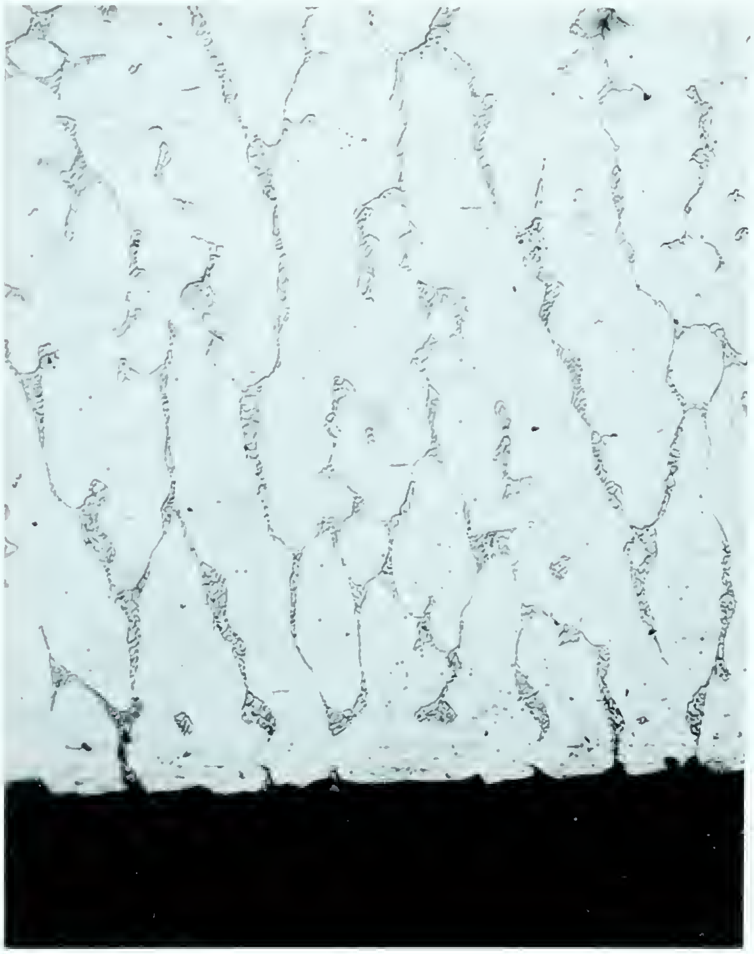

Figure 31. Microstructure of the chill face of an Al - 10% Cu ingot cast in a perpendicular field of 13,000 oersteds, showing the absence of exudations. (X200)

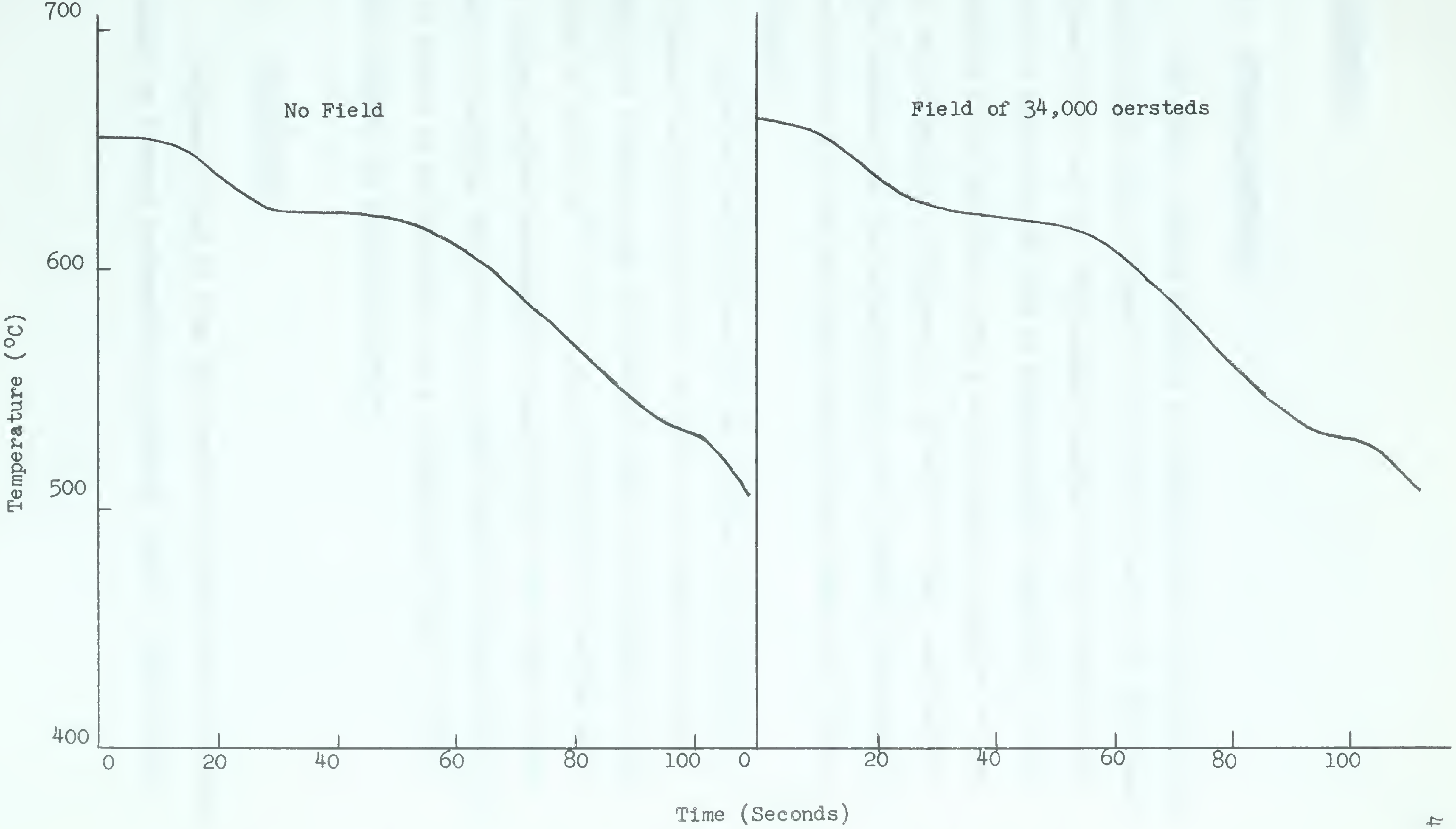

Figure 32 . Comparison of field and no-field cooling curves for Al - 10% Cu ingots .

[illegible]

V. DISCUSSION

A. CRYSTAL MORPHOLOGY

The field, whether parallel or perpendicular to the direction of solidification, had no effect on the columnar growth, as illustrated in Figures 16, 17 and 18. This appears logical in that the field had little or no effect on the rate of solidification (Figure 32). Also, the parallel field had little effect on the dendritic pattern of the ingots as illustrated in Figures 19, 20 and 21. There was, however, a slight tendency for the perpendicular field to disrupt the dendritic pattern (Figure 21), but the effect was small and could be of little significance.

Dendrites usually grow with the crystal axis oriented so as to produce the best heat flow. In most f.c.c. metals, such as aluminum, the dendrites are oriented with the (111) direction in the direction of heat flow(12). It is possible that this direction also has a slightly higher paramagnetic susceptibility than other crystallographic directions, and, if so, one might expect a parallel field to have no effect on the dendrites and a perpendicular field to tend to disrupt slightly the dendritic pattern.

B. SEGREGATION

Figures 26 and 27 show that the field significantly increases the amount of inverse segregation in aluminum (rich) - copper alloys.

The increase over no field results is up to about 60% for a field of 34,000 oersteds. It is interesting to note that the direction of the applied field relative to the direction of solidification appears to have no significance. This is true of the aluminum - copper system because the field has no effect on the cooling rate, but may not be true in alloys of the bismuth — tin and bismuth - antimony systems where the field does have an appreciable effect on the heat conductivity of the system(1).

It is possible to alter the calculated amount of maximum segregation at the chill face by introducing arbitrary changes in the constitutional - specific volume relationship for the alloy system. The change suggested by Colton(1) to account for the segregation increase in the Bi-Sb system, quite apart from the fact that it cannot be theoretically justified, does not agree with the observed segregation in the field - solidified ingots of the aluminum - copper system. The observed segregation can, however, be obtained if the liquidus is shifted to the position shown in Figure 33, while the positions of the specific volume curves remain unchanged. For higher field strengths correspondingly greater shifts of the liquidus curve are required. We shall now attempt to theoretically justify this shift and its implied consequences.

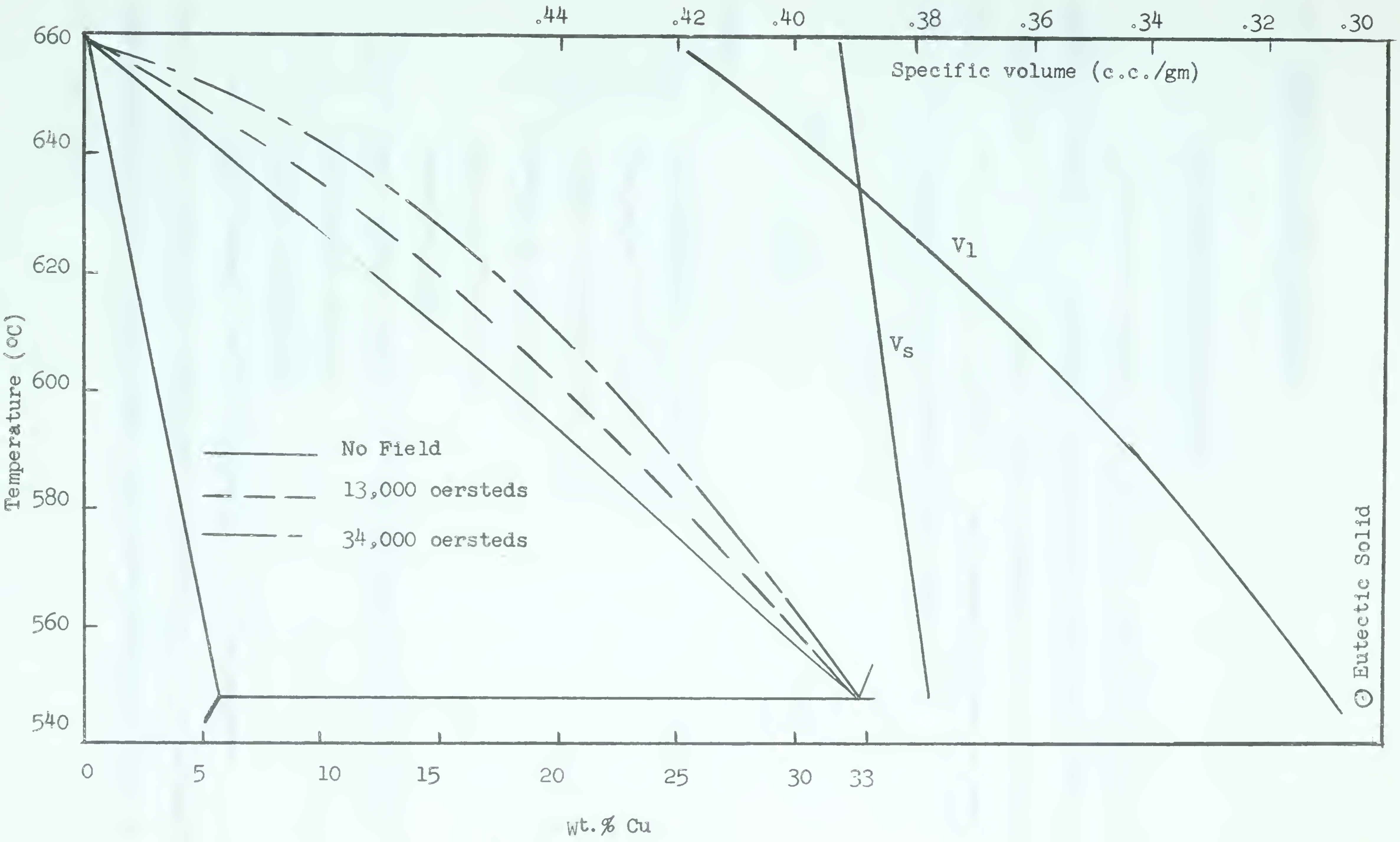

Figure 33. Constitutional diagram and specific volume relationships for the Aluminum (rich) - Copper system.

VI THEORY OF MAGNETIC EFFECTS

A. THERMODYNAMIC CONSIDERATIONS

The effect of a magnetic field on the electronic energy of a weakly paramagnetic or diamagnetic solid derives principally from the diamagnetism of the ion cores and from the diamagnetism and spin paramagnetism of the conduction electrons. The diamagnetic and paramagnetic contributions to the susceptibility are given by (13):

$$\chi_{dia} = -NZ_t\left(\frac{e^2}{6mc^2}\right)\langle r^2\rangle \qquad (11)$$

$$\chi_{para} = \frac{N\mu^2}{3kT} \qquad (12)$$

where:

χ_{dia} = the diamagnetic susceptibility

N = the number of atoms per cubic cm.

Z_t = number of electrons per atom

e = charge of the electron

m = mass of the electron

c = speed of light

$\langle r^2\rangle$ = mean square distance of the electrons from the nucleus

k = Boltzman's constant

T = absolute temperature

μ = approximately the Bohr Magneton 10^{-20} ergs/gauss

There is also a temperature independent contribution to the paramagnetic susceptibility, but it is very small and becomes significant only at very low temperatures.

The energy of a unit mass of material with magnetic susceptibility χ_m (includes all contributions) placed in a magnetic field of strength H, is given by $\frac{1}{2}\mu_0(1+\chi_m)H^2$ (14). This energy is small for weakly diamagnetic and paramagnetic substances, not exceeding a few calories per gm. The change in the heat of solidification of a metal solidified under a magnetic field will, therefore, be:

$$\Delta E = \frac{1}{2}\mu_0(\chi_m^{\ell} - \chi_m^{s})H^2$$

where the superscripts "s" and "ℓ" refer to the solid and liquid respectively. Using aluminum as an example;

$$(\chi_m^{s} = 16.5 \quad , \quad \chi_m^{\ell} = 12.0 \text{ in c.gs. units per gm})^{(22)}$$

the energy change in a field of 34,000 oersteds is 6 X 10^{-6} cals/gm, which is negligible when compared to the heat of solidification of 94 cals/gm. Therefore, this factor will have no observable effect on the constitutional - specific volume relationship of an alloy system.

Another magnetic phenomenon which should be considered is magnetostriction, as a shift of either the specific volume of the liquid or solid in the right direction would tend to increase the amount of segregation. However, magnetostriction is extremely small in alloys other than ferromagnetic alloys and its effects will correspondingly be small and undetectable in segregation work.

Finally, it is necessary to consider the effect of a magnetic field on the solid solubility limits of an alloy system in the sense of the theory of Jones (15), where phase changes in alloy systems occuring at

certain electron/atom ratios are attributed to a lowering of the electronic energy that accompanies the contraction of the Fermi sphere. If the magnetic field were to change the electronic energy of the alloy system, a particular phase change may occur at a different electron/atom ratio and thus at a different composition. A magnetic field does result in the stratification of the electronic states but this stratification has no important consequence except at very huge fields in the order of 100,000 oersteds, and even then the effect is only to cause slight oscillations in electric and magnetic properties as manifested by the de Haas van Alphen effect (16). Therefore, the magnetic field should have no effect on the solubility limits of an alloy system. This is substantiated experimentally by the presence of coring in the solid dendrites.

The above discussion suggests that the magnetic field strengths used in this investigation have little or no effect on the solubility limits of an alloy system and accordingly we look elsewhere for an explanation.

B. THE PLASMA CONCEPT OF A METAL

In its original and narrower sense, the term plasma is applied to an ionized gas having a nearly equal number of positive and negative charges (17). In a much broader sense, the term plasma is taken to mean a gas of charges embedded in a region of opposite charge to maintain electrical neutrality. Thus, a solid or liquid metal can be considered to have plasma - like properties by virtue of the free or conduction

electrons, particularly the liquid because of the high degree of translational freedom of the ion cores which is absent in the solid.

A density or pressure gradient in a plasma under the influence of a magnetic field is responsible for various drift motions, which in the absence of collisions is perpendicular to both the field (H) and the pressure gradient ($\vec{\nabla} P$). Collisions between electrons and ions will result in a diffusion flow component parallel to $\vec{\nabla} P$. The velocity of this motion transverse to the lines of force is given by:[18]

$$V_\perp = \frac{\vec{H}}{\mu H^2} \times \left(-E + \frac{\vec{\nabla} P_i}{e n_e} \right) - \left(\frac{1}{\sigma_\perp \mu^2 H^2} \vec{\nabla} P \right) \qquad (13)$$

where:

H - field strength

μ - permeability

E - internal electrical field

$\vec{\nabla} P_i$ - pressure gradient of ion cores

e - electronic charge

n_e - density of electrons

$\sigma_\perp$ - conductivity transverse to field direction

$\vec{\nabla} P$ - total pressure gradient

This net drift along the pressure gradient is primarily due to collisions between electrons and positive ions since the reciprocal conductivity term is related to the rate of momentum transfer to ions from the electrons.

It is not possible to compare the components of flow velocity along $\vec{\nabla}$ P in equation (13) to normal diffusion velocities in liquid metals because of their essentially different natures. The pressure gradient in (13) arises mainly from the field and the "diffusion" is flow resulting from the motion of cores and electrons together, not movement of one species relative to another as in ordinary diffusion. Equation (13) does, however, show the nature of diffusion inhibition. The mass transfer associated with the density gradient has two components, one perpendicular to the gradient and one parallel to it, the extent of parallel flow being inversely proportional to H^2 and the conductivity $\sigma_\perp$.

The effect of the magnetic field is to cause a gyration of the free electrons in the liquid metal. If the gyration radius (r) is less than the normal mean free path of the electron, (λ), a drift velocity perpendicular to the density gradient will result and "diffusion" along the density gradient and transverse to the lines of force will be slight, arising only from collisions of the guiding centres. It is not clear to what extent the situation $r<\lambda$ can be approached in liquid metals but providing the situation is approached, electron motion across the lines of force would be largely immobilized and the heavy positive ions would be confined by the electric field set up the slight deviation from electrical neutrality, thus greatly inhibiting diffusion.

C. DIFFUSION INHIBITION AND ITS CONSEQUENCES

As suggested previously in this discussion, the amount of segregation in field-solidified ingots can be obtained by calculation, providing the liquidus line is raised to the positions shown by the dotted lines in Figure 33. An attempt will be made to justify this change in the constitutional diagram by considering the effect of the magnetic field on the solute concentration gradient ahead of an advancing solid - liquid interface.

The concentration gradient ahead of an advancing interface is shown schematically in Figure 34. If the magnetic field inhibits diffusion of the solute atoms, the mass transfer will tend to change from a diffusion process to one of forced convective flow. This will

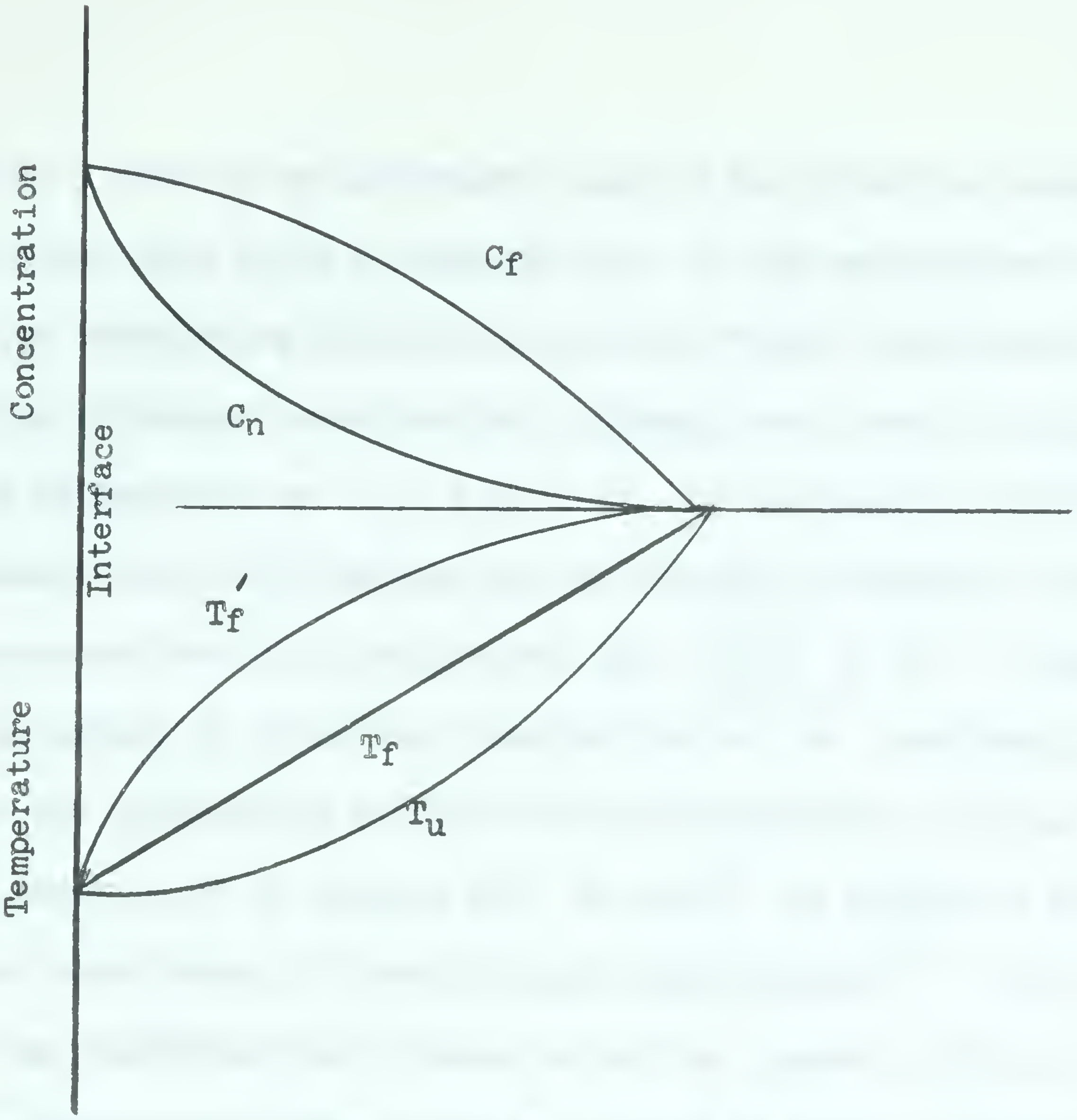

C_n - Normal concentration gradient in liquid

C_f - Proposed concentration gradient due to field

T_u - Solidification temperature for C_f using unchanged constitutional diagram

T_f and T_f' - Solidification temperatures for C_f obtained by raising the liquidus line of the constitutional diagram.

Figure 34. - Concentration gradients and temperature distribution at the solid - liquid interface.

result in a pile up of the solute atoms at the interface changing the distribution from C_n to C_f (Figure 34). If the equilibrium solidification temperature is plotted for this "field" concentration curve using the unchanged constitutional diagram, one obtains a curve similar to that illustrated by T_u in Figure 34. An equilibrium solidification temperature such as T_u (Figure 34) is, however, contrary to the principles of heat flow which state that $\frac{d^2T}{dx^2} \leq 0$. Therefore, it is necessary to raise the liquidus line of the constitutional diagram so that the equilibrium solidification temperature is lowered at least to the position of T_f (Figure 34), or even T_f' as dendritic growth requires some degree of constitutional supercooling (3). Therefore, in order for solidification to occur under the imposed diffusion constraint, the constitutional diagram must be altered as shown in Figure 33.

D. ENERGY CONSIDERATIONS

Having proposed that the magnetic field changes the form of the constitutional diagram via diffusion inhibition, it remains to reconcile this change with the concept of local equilibrium of irreversible thermodynamics.

The cohesive energy of a lattice (and we include here the liquid state) can in principle be accurately represented through the Schrödinger wave equation for the system. The equation, as such, is mathematically intractable except for the simplest of systems. Approximation methods are necessary to treat the more complicated

problems, the cellular approximation method of Wigner and Seitz(19) being the most successful so far. However, even this method is accurate only for the more simple alkali metals. Nevertheless, it has also be applied (with appropriate modifications) to bi- and multi- valent metals with some success.

The cohesive energy of a lattice referred to its sublimated state is given by(20)

$$-E_I = E_0 + \frac{3}{5}\frac{h^2}{m}\left(\frac{9}{4\pi^2}\right)^{2/3} \cdot \frac{Z^{2/3}}{r_0^2} + \frac{be^2}{r_0} \qquad (14)$$

where

E_0 = the zero point energy of the electron in the lattice
h = Planck's constant
m = mass of the electron
Z = valence of the metal
r_0 = radius of the unit cell in the sphere approximation

The second term is the average Fermi energy of the electrons, and the third term accounts for the average electron interaction energy per electron pair in any one atomic cell, which involves the electron exchange and correlation energies.

Since r_0 is proportional to $V_0^{1/3}$, the total energy of a lattice is frequently represented by the equation

$$E_I = A\left(\frac{V}{V_0}\right) + B\left(\frac{V}{V_0}\right)^{2/3} + C\left(\frac{V_0}{V}\right)^{1/3} \qquad (15)$$

where A, B and C are constants for the particular system. Equation (15) emphasizes the dependence of cohesive energy on the atomic volume (or interatomic distance). The activity of a component atom, which is determined by its contribution to the cohesive energy of the lattice, is, therefore, strongly dependent on the atomic volume, hence also on the specific volume.

In alloy formation it is usually assumed that the free electrons exist in two bands associated with the potential fields of the constituent ions. If the energy levels of the two bands are different, there will be a redistribution of electrons between bands to lower the total energy by an amount equal to the bond energy. Beardeen and Friedman (21) have observed changes in widths of the Fermi bands during alloying of copper and zinc indicating that the zinc band, i.e., those electrons in the zinc cells, decreases on the high energy side with increased dilution of zinc.

The proposed shift of the liquidus curve per se represents a departure from local equilibrium and, therefore, an increase in energy. However, it is suggested that this is counterbalanced by the energy change involved in a proposed volume change (Equation (15)) which derives from a redistribution of the electrons between the solute and solvent cells. Thus, local equilibrium can be restored at the interface through the process of specific volume increase or decrease.

This alteration of the constitutional - specific volume relationship by the field is such that the temperature-density

relationship immediately adjacent to the interface is assumed not to change from its equilibrium value. This is only an approximate average of the situation in the region of the interface because:

1) the segregation calculations are based on the assumption that the interdendritic liquid for constant height of the ingot is homogeneous, which is no longer true for field solidified ingots.

2) only growth directions perpendicular to the direction of the magnet field are affected which would involve only about 50% of the mass.

The most that can be said for the altered phase diagram is that it represents the approximate integrated effect of the field.

VII SUMMARY AND CONCLUSIONS

(1) The effect of the magnetic field is to increase the amount of inverse segregation in aluminum (rich) - copper alloys. The amount of segregation increases with increasing field strength, and is 60% higher than the no-field results for a field strength of 34,000 oersteds.

(2) Fields both parallel and perpendicular to the direction of solidification of similar strengths increased the segregation by similar amounts.

(3) Neither the parallel field nor the perpendicular field had any effect on the columnar growth characteristics and the cooling rates of the alloys.

(4) When the field was applied perpendicular to the direction of solidification, there was a slight tendency for the dendritic pattern to be disturbed.

(5) A theory introducing the concept of diffusion inhibition in the liquid by the magnetic field has been proposed in order to justify the alteration of the phase diagram. The theory is compatible with the heat flow requirements and energy considerations for the solidifying system.

BIBLIOGRAPHY

1. D. R. Colton, Master's Thesis, University of Alberta (1960)
2. J. S. Kirkaldy and W. V. Youdelis, AIME Trans. 212, 833, (1958)
3. B. Chalmers, AIME Trans. 200, 519 (1954)
4. F. C. Frank, Farady Soc. Disc., No. 5, 48 (1949)
5. W. G. Pfann, Liquid Metals and Solidification, A.S.M. (1958)p. 218
6. V. G. Smith, W. A. Tiller, and J. W. Rutter, Can. J. Phys. 33, 723 (1955)
7. W. A. Tiller and J. W. Rutter, Can. J. Phys. 34, 96 (1956)
8. S. M. Daniels, Proc. Phys. Soc. B, 63, 1028 (1950)
9. K. A. Jackson, Liquid Metals and Solidification, A.S.M. (1958) p. 174
10. O. Snellman and F. J. Burge - J. Sci. Inst., 26, 331 (1949)
11. W. W. Scott, Standard Methods of Chemical Analysis, Vol. 1, D. Van Nostrand Company Inc. (1939) p. 40, 368
12. W. C. Winegard, Metallurgical Rev. No. 6, 57 (1961)
13. A. J. Dekker, Solid State Physics, Prentice - Hall, Inc., (1961) p. 446
14. J. R. Reitz and F. J. Milford, Foundations of Electromagnetic Theory, Addison - Wesley Publishing Co. Inc., (1960) p. 194, 235
15. H. Jones , Proc. Roy. Soc., A 144, 225 (1934)
16. W. de Haas, and P. M. van Alphen, Leid. Comm., 212a (1931)
17. I. Langmuir, Phys. Rev., 33, 954 (1929)

18. L. Spitzer, Physics of Fully Ionized Gases, Interscience Pub. Inc., New York, 24 (1957)

19. E. Wigner and F. Seitz, Phys. Rev., 43, 804 (1933)

20. A. H. Wilson, The Theory of Metals, Cambridge Univ. Press (1954) p. 74

21. J. A. Beardeen and H. Friedman, Phys. Rev., 58, 387 (1940)

22. Handbook of Chemistry and Physics, 44th Edition,(1962-63) p. 2731

23. W. V. Youdelis, and D. R. Colton, Trans. AIME, 218, 628 (1960)

APPENDIX

THE CALCULATION OF INVERSE SEGREGATION

The underlying assumptions used in the derivation of the inverse segregation are:

(1) the flowback of residual liquid is complete so that no shrinkage porosity occurs

(2) local equilibrium exists at the solid - liquid interface

(3) the interdendritic liquid is homogeneous at any particular height of the ingot, i.e., the interdendritic spacing is considered small enough so that no concentration gradients exist between dendrites.

(4) solidification is unidirectional, and

(5) solid coring is complete, i.e., solidification is rapid enough so that there is no diffusion in the solidified alloy.

Definition of terms:

m_s = mass of solidified metal

m_ℓ = mass of liquid metal

a = contraction coefficient upon solidification

c_ℓ = concentration of the liquid metal

C_s = concentration of the cored crystals

The subscript "e" refers to the eutectic temperature.

The calculation is given for an alloy system which has a eutectic - type phase diagram but the theory is applicable to systems

which have other type phase diagrams, e.g., the bismuth - antimony (1) system which exhibits complete solid solubility, and the aluminum - zinc system (23) .

The amount of segregation for a eutectic system is given by the equation:

$$\Delta C = \frac{\frac{c_{le} m_{le}}{a_e} + C_{se} m_{se}}{m_{le}/a_e + m_{se}} - C_o \qquad (1)$$

The term m_{le} is the mass of liquid of eutectic composition and is obtained from the equation

$$\frac{dm_l}{m_l} = -\frac{a}{A}\frac{dC_l}{C_l} \qquad (2)$$

where

$$a = \frac{c_l - c_s}{V_L}\frac{dV_L}{dc_l} + \frac{V_s}{V_L}$$

and

$$A = \frac{C_l - C_s}{C_l}$$

where C_l and C_S are the concentrations of liquid and solid at a given temperature and V_L and V_S are the corresponding specific volumes.

Therefore

$$m_l^{i+1} = m_l^i \left(\frac{C_l^{i+1}}{C_l^i}\right)^{-\frac{a^i}{A^i}} \qquad (3)$$

The term m_{se} is the mass of the cored primary dendrites and is obtained from the equation

$$dm_s = -\frac{dm_l}{a} \qquad (4)$$

Therefore:

$$m_s^{i+1} = m_s^i + \frac{m_l^i - m_l^{i+1}}{a^i} \qquad (5)$$

The term $C_{se} m_{se}$ is the amount of copper in the cored primary dendrites and is obtained from the equation:

$$C_s^{i+1} m_s^{i+1} = C_s^{i} m_s^{i} + \left(\frac{1 - A^i}{A^i - a^i} \right) m_\ell^i C_\ell^i \left[\left(\frac{C_\ell^{i+1}}{C_\ell^{i}} \right)^{\frac{A^i - a^i}{A^i}} - 1 \right] \qquad (6)$$

The superscripts i and $i+1$ refer to the i^{th} and $i+1^{th}$ terms respectively in the stepwise integration since a and A are usually functions of the solute concentration. The summation of the terms in (3), (5) and (6) is taken to the eutectic temperature to obtain the terms $m_{\ell e}$, m_{se} and $C_{se} m_{se}$.

B29805